BACHELOR'S DEGREE THESIS

Degree in Mathematics

Title: Computation of Lagrangian Coherent Structures with Application to Weak Stability Boundaries

Author: Xavier Ros Roca

Advisor: Francesco Topputo

Department: Dipartamento di Scienze e Tecnologie Aerospaziali, Politecnico di Milano

Co-Advisor: Mercè Ollé Torné

Department: Departament de Matemàtica Aplicada I

Academic year: 2014 - 2015

UNIVERSITAT POLITÈCNICA DE CATALUNYA
BARCELONATECH
Facultat de Matemàtiques i Estadística

Universitat Politècnica de Catalunya
Facultat de Matemàtiques i Estadística

Bachelor's Degree Thesis

Computation of Lagrangian Coherent Structures with Application to Weak Stability Boundaries

Xavier Ros Roca

Advisor: Francesco Topputo[1]
Co-advisor: Mercè Ollé Torné[2]

1. Dipart. di Scienze e Tecnologie Aerospaziali - Politecnico di Milano
2. Departament de Matemàtica Aplicada I - UPC

Als meus avis,
als dos els hauria agradat
llegir aquesta tesi

Abstract

Key words: ordinary differential equations, non-linear dynamics, Lagrangian coherent structures, celestial mechanics, elliptic three body problem

MSC 2010: 34C99, 37C10, 70F07, 70F15, 70K99

Real-life mechanical systems can usually be modeled as non-linear, non-periodic and non-autonomous dynamical systems. It is very important to have different tools to study these systems, and there are many classical procedures developed for this purpose. During the last decade, a new tool has been introduced, the Lagrangian Coherent Structures (LCS). They represent the most repelling and attracting structures of the phase space. Roughly speaking, LCS are particular manifolds that separate regions of space with distinctly different dynamics. In this thesis, algorithms to find the LCS of a system are presented and finally they will be applied in the *Elliptic Restricted Three Body Problem* in Astrodynamics in order to identify the *Weak Stability Boundaries*.

Acknowledgements

First of all, I would like to thank my advisors in Politecnico di Milano, Francesco Topputo and Alex Wittig. They invested a lot of their time in this thesis, meeting every Tuesday. I am very grateful to them for their scientific support and their warm host during these 6 months in Milan. Grazie mille!

També vull agrair profundament a la Mercè Ollé, professora de la Univeristat Politècnica de Catalunya i co-tutora d'aquest Treball de Fi de Grau, per donar-me l'excel·lent contacte del Francesco a Milà. Valoro molt també la lectura desinteressada amb ull crític de la tesi per part seva.

Quiero agradecer también a Ana, Mario e Inés por las horas invertidas en el proyecto en la sala de tesistas en Milán, el *hacer un café* de media mañana, el *tris* para comer en la cafetería de Bovisa y también que me acogieran siempre en Ingegnoli 5 cenando el mejor *kebab* de Milán.

Vull fer especial menció als meus companys de carrera, tant el grup de Findus com els amics de la FME i de l'ETSEIB, per aquests magnífics 5 anys universitaris i les mil experiències viscudes. Així com al CFIS i el seu equip directiu i administratiu per la oportunitat i dedicació durant aquests anys.

La major part del TFG ha estat elaborada a Milà, per tant, vull donar les gràcies també als amics d'Erasmus com la Laura, l'Alba i el Carlos amb el nostre magnífic viatge i, sobretot, a Carolina y Fer por su buena amistad y grandes momentos en Milán, habéis sido una pieza fundamental.

Finalment, fer especial menció a gent que m'ha ajudat molt durant l'elaboració del TFG com l'Uri Castejón, amb la resolució de dubtes tècnics en sistemes dinàmics, a la Paula, pels infinits Hangouts Amsterdam-Milà i a la Marina per hores d'escriptura junts i consells tècnics. Sense oblidar-me òbviament dels meus pares, la meva germana i gent molt especial com l'Albert, l'Anna, el Jaume, la Glòria i el Raül i un llarg etcètera. Gràcies a tots de debò!

Contents

1 Introduction

This chapter introduces the main topic of this thesis, the *Lagrangian Coherent Structures*. The motivations for studying this new field in non-linear dynamical systems will be given. Secondly, some research history will be explained and to finish this chapter, there will be some preliminary definitions and results of Dynamical Systems.

1.1 Motivation

The study of Dynamical Systems, the study of their behavior with respect to initial conditions, in the case of autonomous, time-periodic and quasi-periodic systems is very complete and rigorous. In those systems, one can study the fixed points, the invariant manifolds and, from these invariant objects, one can also study the qualitative behavior of all the system.

In contrast, all these techniques are not applicable in non-autonomous and aperiodic systems and the reality is that no fluid particle in the ocean or atmosphere will be part of a periodic orbit. Historically, there are many procedures such as linearization or modern heuristic diagnostics to try to obtain some information of the Lagrangian point of view of these systems, [9].

This thesis studies a new technique to try to understand the real-life systems mathematically. This new approach tries to show the transport pattern of the system through the most repelling, attracting and shearing structures of the system. These structures will be what is called *Lagrangian Coherent Structures*, shortly LCS. An LCS must act as separatrix of regions with qualitatively different dynamics, [13]. To turn this characteristic to a mathematical definition took many years and approaches that are shown in this thesis.

The applications in fluid dynamics of this new concept are remarkable. In 2010 two globally significant events occurred. In April, a volcanic eruption in Iceland caused chaos in the European airspace. The same month, there was an explosion in the Gulf of Mexico causing the largest offshore oil spin in the US. In addition, in March 2011, a tsunami in Japan caused a nuclear-reactor disaster and the release of amounts of radioactive contamination in the Pacific ocean. As explained in [18], further analysis showed that finding the attracting and repelling LCS of these three significant events would have been useful to forecast future situations of the disasters and to take better decisions. This informative article ensures that LCS will be a very powerful

tool when computation and data storage improve in many fields such as biological fluids, industrial and chemical transports.

One last objective of this thesis is to find a new application of LCS in Astrodynamics. The repelling Lagrangian coherent structures will be used as an alternative to find the *Weak Stability Boundaries* (WSB) in the *elliptic restricted three body problem* (ER3BP). Roughly speaking, WSB is a *boundary of a region near the planet where capture of the third particle occurs*, [21]. This technique was developed during the 80s and proved in 1991 when Japanese satellite Hiten was able to reach the Moon, [21]. The WSB is useful to find what it is called as *low-cost* transfers to reach a planet, [2], because the particle is *ballistically captured*, ie, the object makes, under natural dynamics within the sphere of influence of that planet, at least one complete revolution around the planet, [12].

1.2 Brief History of LCS

At the beginning, the aim of the researchers that work on this topic was to find what they named as the *skeleton* of the fluid, which are some structures that will give an idea of the pattern and shape of the flow after an interval of time. The term of *Lagrangian coherent structure* was coined by *G. Haller* and *G. Yuan* in [10] in 2000. This name was used for defining the most attracting and repelling material surfaces of the system. The immediate application of this new concept is to find some separatrices in the phase space, in the case of the most repelling structures, or to find, for example, the area where there will be more concentration of a substance after a while, in the case of the attracting LCS.

A lot of theories have been developed during these 15 years, [7, 8, 15]. The main researchers and developers are *George Haller* and his research group established in Zurich, *Thomas Peacock* from MIT and *Shawn Shadden* from Berkeley University. Those last two researchers dedicated their research on stochastic dynamical systems and *G. Haller* works on continuous dynamical systems focused on unsteady flows.

From 2005 to 2010, LCS has not had a mathematical definition. Firstly they were defined as the ridges of *Finite-Time Lyapunov Exponents* field (FTLE), [8, 15], but in 2010, *G. Haller* in [8] realized that FTLE field ridges were not corresponding to the repelling LCS and turned the physical definition into a mathematical definition. Furthermore, he developed a mathematical, and rigorous, theory of LCS around the invariants of Cauchy-Green strain tensor field. In this remarkable paper, he also established the sufficient and necessary conditions for the existence of LCS and a new way to find them.

From 2010, their research is focused on new theory in higher-dimensional flows and on obtaining new efficient methods to find LCS, [3, 5, 6, 9]. The future research has to be focused on finding an efficient implementation to ease the obtaining of LCS because it will be a useful tool to forecast future states in all kind of flows.

1.3 Introduction to Dynamical Systems

The main definition of a Dynamical System is taken from [17], which defines it as a *rule* for time evolution on a state phase, using more formal vocabulary:

1.3.1 Definition (Dynamical System) A *Dynamical System* is a system that evolves in time. This system is formed by a state space S, a set of times T and a rule $R : S \times T \to S$ which describes the evolution of the state in time.

The *state space* is a set of coordinates needed to describe completely the system. This space is going to change in time, so the *rule* will predict the next state or states. It can be discrete or continuous. When it's continuous, it is usually a smooth manifold into $\mathbb{R}^n$ and it's called *phase state*.

The *set of times* can be also discrete, for example in an ideal coin toss dynamics, or continuous. In the case of being continuous, it can be assumed as an interval $I = [\alpha, \beta] \subseteq \mathbb{R}$.

Finally the *rule* is an application that describes the future state or states of a coordinate in S. For a state $s_0 \in S$, the *orbit* or *trajectory* is the time-ordered sequence of states using the *rule*.

Along this thesis, LCS are studied only in Dynamical Systems where the state space and the time space are both continuous. Furthermore, the phase state should be a manifold into a finite dimensional space. One can model these systems as a general Ordinary Differential Equations' Cauchy problem:

$$\begin{cases} \dot{\mathbf{x}}(t) &= \mathbf{f}(\mathbf{x}(t), t) \\ \mathbf{x}(t_0) &= \mathbf{x}_0 \\ \mathbf{x}(t) &\in \Omega \subseteq \mathbb{R}^n \\ t &\in I = [\alpha, \beta] \end{cases} \tag{1.1}$$

where t is the independent variable that represents the time and $\mathbf{x}(t)$ represents the state of the system at time t. The field $\mathbf{f} : \Omega \times I \to \Omega$ is a sufficiently smooth field called the *velocity map*. Traditional assumptions in fluid mechanics, [20], ask to $\mathbf{f}(\mathbf{x}(t), t)$ to be at least C^0 in time and C^2 in space. From that, it follows that the flow $\boldsymbol{\phi}_{t_0}^t(\mathbf{x})$ will be C^1 in time and C^3 in space.

Equivalently, one can define the evolution of a Dynamical System through the *flow map*, which is defined below.

1.3.2 Definition (Flow map) For $t_0, t \in I$, we can define the flow map as

$$\begin{aligned} \boldsymbol{\phi}_{t_0}^t : \quad \Omega &\to \quad \Omega \\ \mathbf{x}_0 &\mapsto \quad \boldsymbol{\phi}_{t_0}^t(\mathbf{x}_0) = \mathbf{x}(t; t_0, \mathbf{x}_0) \end{aligned}$$

The *flow map* satisfies the following properties for any $\mathbf{x} \in \Omega$:

1) Identity

$$\boldsymbol{\phi}_{t_0}^{t_0}(\mathbf{x}) = \mathbf{x}$$

2) Group property

$$\boldsymbol{\phi}_{t_0}^{t+s}(\mathbf{x}) = \boldsymbol{\phi}_{s}^{t+s}(\boldsymbol{\phi}_{t_0}^{s}(\mathbf{x})) = \boldsymbol{\phi}_{t}^{t+s}(\boldsymbol{\phi}_{t_0}^{t}(\mathbf{x}))$$

3) Differentiability

$$\frac{\mathrm{d}\boldsymbol{\phi}_{t_0}^{t}(\mathbf{x})}{\mathrm{d}t} = \mathbf{f}(\mathbf{x}(t), t)$$

1.3.3 Proposition (Variational equations) Consider any initial conditions $x_0 \in \Omega$ and $t \in I$ in a Dynamical System of the form of (1.1). Then, given a fixed time $t \in I$, the following ordinary differential equations system is satisfied, recalling

$$\Phi := \Phi(t; t_0, \mathbf{x}_0) = D_{\mathbf{x}_0}\boldsymbol{\phi}_{t_0}^{t}(\mathbf{x}_0) \quad , \quad \mathbf{A}(\mathbf{x}, t) = D_{\mathbf{x}}\mathbf{f}(\mathbf{x}, t)$$

then

$$\begin{cases} \dot{\Phi} & = & \mathbf{A}(\mathbf{x}, t)\ \Phi \\ \Phi(t_0; t_0, \mathbf{x}_0) & = & \mathbf{Id}_n \end{cases}$$

where $\mathbf{Id}_n$ is the n-dimensional identity matrix, $\Phi = \Phi(t; t_0, \mathbf{x}_0)$ is the *state transition matrix* of the system and $\mathbf{A}$ is the Jacobian of the velocity field.

If one joins the two systems

$$\begin{cases} \dot{\mathbf{x}}(t) & = & \mathbf{f}(\mathbf{x}(t), t) \\ \mathbf{x}(t_0) & = & \mathbf{x}_0 \\ \mathbf{x}(t) & \in & \Omega \subseteq \mathbb{R}^n \\ \dot{\Phi} & = & \mathbf{A}(\mathbf{x}, t)\ \Phi \\ \boldsymbol{\Phi}(t_0; t_0, \mathbf{x}_0) & = & \mathbf{Id}_n \\ t & \in & I = [\alpha, \beta] \end{cases} \tag{1.2}$$

This system is called the *Variational equations* of the system and it is $n+n^2-$dimensional. The variational equations are useful to find the Jacobian of the flow, Φ, that will be essential in this thesis.

1 Proof The flow satisfies the differential equation (1.1), so we have

$$\frac{\mathrm{d}}{\mathrm{d}t}\boldsymbol{\phi}_{t_0}^{t}(\mathbf{x}_0) = \mathbf{f}\left(t, \boldsymbol{\phi}_{t_0}^{t}(\mathbf{x}_0)\right)$$

By deriving the equality with respect to the initial condition $\mathbf{x}_0$

$$D_{\mathbf{x}_0}\left[\frac{\mathrm{d}}{\mathrm{d}t}\boldsymbol{\phi}_{t_0}^{t}(\mathbf{x}_0)\right] = D_{\mathbf{x}}\left(\mathbf{f}\left(t, \boldsymbol{\phi}_{t_0}^{t}(\mathbf{x}_0)\right)\right) D_{\mathbf{x}_0}\boldsymbol{\phi}_{t_0}^{t}(\mathbf{x}_0)$$

By Cauchy-Schwarz theorem, the derivatives order in the left hand side can be changed

$$\frac{\mathrm{d}}{\mathrm{d}t}\left[D_{\mathbf{x}_0}\boldsymbol{\phi}_{t_0}^{t}(\mathbf{x}_0)\right] = D_{\mathbf{x}}\left(\mathbf{f}\left(t, \boldsymbol{\phi}_{t_0}^{t}(\mathbf{x}_0)\right)\right) D_{\mathbf{x}_0}\boldsymbol{\phi}_{t_0}^{t}(\mathbf{x}_0)$$

so then, as wanted

$$\dot{\Phi} = \mathbf{A}(\mathbf{x}, t) \cdot \Phi$$

For the initial condition, it's only necessary to derive the first property of the flow with respect to the initial conditions

$$D_{\mathbf{x}_0}\boldsymbol{\phi}_{t_0}^{t_0}(\mathbf{x}_0) = D_{\mathbf{x}_0}(\mathbf{x}_0) \iff \Phi(t_0; t_0, \mathbf{x}_0) = \mathbf{Id}_n$$

□

One important object in this thesis is the *finite-time Cauchy-Green strain tensor* which shows the average deformation of the infinitesimal neighborhood after a finite-time interval. As an operator, it will be a very useful tool to find the maximum stretching direction at every point.

1.3.4 Definition (Finite-time Cauchy-Green strain tensor) Let $\mathbf{x}_1(t_0) \in \Omega$ be a particle in the phase space and $\mathbf{x}_2(t_0) = \mathbf{x}_1(t_0) + \delta\mathbf{x}(t_0)$ at the initial time. After a time interval T, these points will be $\mathbf{x}_1(t_0+T)$ and $\mathbf{x}_2(t_0+T)$. Then, by first order Taylor expansion,

$$\delta\mathbf{x}(t_0+T) = \boldsymbol{\phi}_{t_0}^{t_0+T}(\mathbf{x}_2) - \boldsymbol{\phi}_{t_0}^{t_0+T}(\mathbf{x}_1) = \Phi \cdot \delta\mathbf{x}_0 + \mathcal{O}(\|\delta\mathbf{x}_0\|^2)$$

where Φ is the state transition matrix for a finite time t_0+T. The norm of this vector $\delta\mathbf{x}(t_0+t)$ indicates the distance of the two particles after T.

$$\|\delta\mathbf{x}(t_0+T)\|^2 = \langle \Phi\cdot\delta\mathbf{x}_0, \Phi\cdot\delta\mathbf{x}_0\rangle = \ \delta\mathbf{x}_0^T\cdot\Phi^T\cdot\Phi\cdot\delta\mathbf{x}_0 = \delta\mathbf{x}_0^T\cdot\Delta\cdot\delta\mathbf{x}_0$$

where the Cauchy-Green tensor is $\Delta(T;\mathbf{x}_0,t_0) := \Phi^T\cdot\Phi$. The notation $\Delta := \Delta(t_0+T;\mathbf{x}_0,t_0)$ and $\Phi := \Phi(t_0+T;\mathbf{x}_0,t_0)$ will be used along all the thesis.

By construction, one can easily see that Δ is symmetric and positive definite because it comes from a distance definition. Thus, it has n real positive eigenvalues that can be ordered as

$$0 < \lambda_1 \leq \cdots \leq \lambda_n$$

These n eigenvalues and their n associated eigenvectors indicate the stretching magnitude on each direction. When $\lambda_i < 1$, the system is compressing at the associated direction. Otherwise, when $\lambda_i > 1$, the system is expanding. The maximum stretching will be at the associated eigenvector $\boldsymbol{\xi}_n$ of the maximum eigenvalue, λ_n.

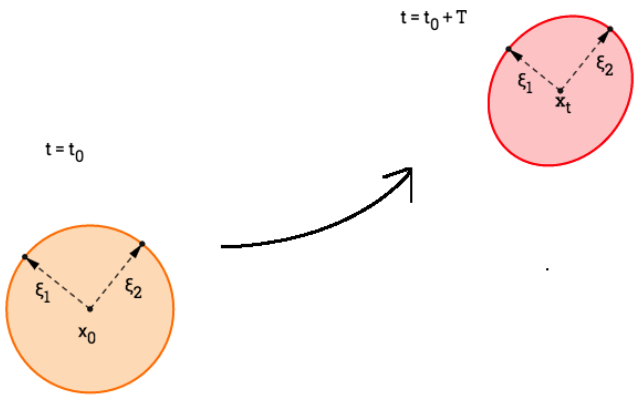

Figure 1.1: Ellipsoid of the Cauchy-Green tensor in a $2D-$system. The length of the unit vectors $\boldsymbol{\xi}_1$ and $\boldsymbol{\xi}_2$ become $\sqrt{\lambda_1}$ and $\sqrt{\lambda_2}$ respectively after the time interval.

Further information of the system can be extracted from this tensor. Due to the fact that the tensor is symmetric and positive definite, the eigenvectors are orthogonal and they turn the infinitesimal sphere around $\mathbf{x}_0$ into an ellipsoid as in Figure 1.1. Moreover, one can notice that the system is area-preserving when the product of all the eigenvalues is equal to 1, expanding when it is greater than 1 and compressing when it is less than 1.

One last definition is needed for this thesis. This is the notion of *material surface*.

1.3.5 Definition (Material surface) A *Material surface* is denoted by $\mathcal{M}(t)$ and it is a manifold of the phase space $\Omega \times [\alpha, \beta]$, generated by the advection of an $n-1$-dimensional manifold $\mathcal{M}(t_0) \subset \Omega$ by the flow map. So then:

$$\mathcal{M}(t) = \boldsymbol{\phi}_{t_0}^{t}(\mathcal{M}(t_0))$$

Equivalently, and more understable, one *Material surface* is one manifold of the phase space at the initial time, $\mathcal{M}(t_0)$, that is advected by the flow until a finite time. Hence, $\mathcal{M}(t_0)$ is evolving with the flow. Since $\boldsymbol{\phi}_{t_0}^{t}$ is a diffeomorphism, the material surface at time t is as smooth as the initial surface $\mathcal{M}(t_0)$ and it is $n-1$-dimensional, $\forall t$.

As shown in next chapter, an LCS must be a material surface as it is written in Proposition 2.1.1.

2
Lagrangian coherent structures

The aim of this chapter is to collect all the theory developed around the LCS. The historical development of the theory will be followed in this chapter. Therefore, first the Finite-Time Lyapunov Exponent (FTLE) field and it's relation with the LCS is introduced, followed by the newer Variational LCS theory.

This chapter is very influenced by [8] where *G. Haller* makes a deep review of the theory obtained until 2010 and develops rigorously the Variational LCS theory, which corresponds to Section 2.3 in this thesis.

2.1 Characteristics of an LCS

Complex dynamical systems are usually very sensitive to changes in their initial conditions. This makes the classification of dynamical regimes where orbits behave similarly hard to do by the classical methods. Behind these complex and sensitive patterns, however, there exists a robust skeleton of special material surfaces called *Lagrangian coherent structures*.

The world *Lagrangian* comes from the fact that these structures must evolve with the flow, as a material surface does. The words *coherent structures* mean that they are regions of the flow that are distinguishable in time and space and separate different dynamics of the flow.

First results in LCS theory demonstrate that these structures were full separatrices in the phase space through the time. Nevertheless, more recent investigations, [13, 15, 20], show that particles can cross the LCS and therefore that LCS separate regions that have qualitatively different dynamics. That is, LCS act as the most important barriers to mixing of scalar fields such as dye concentrations in fluids.

2.1.1 Proposition As proposed in [10], LCS are expected to have two key properties:

1) An LCS should be a material surface, as given in 1.3.5, because it must have sufficient dimension to have a visible impact and must move with the flow to act as a transport barrier.

2) An LCS should present locally the strongest attraction, repulsion or shearing forces in the flow.

Recalling classical invariant manifolds classification in autonomous dynamical systems, LCS can also be classified in three categories:

- *Hyperbolic LCS*: The most attracting and repelling structures.
- *Elliptic LCS*: Closed material surfaces.
- *Parabolic LCS*: The strongest shearing structures.

In this thesis, only hyperbolic LCS are going to be studied in depth.

Based on the key properties that an LCS must satisfy, one can give a purely physical definition:

2.1.2 Definition (Physical Definition of Hyperbolic LCS) A Hyperbolic LCS over a finite time-interval $I = [\alpha, \beta]$ is a locally strongest repelling or attracting material surface over I.

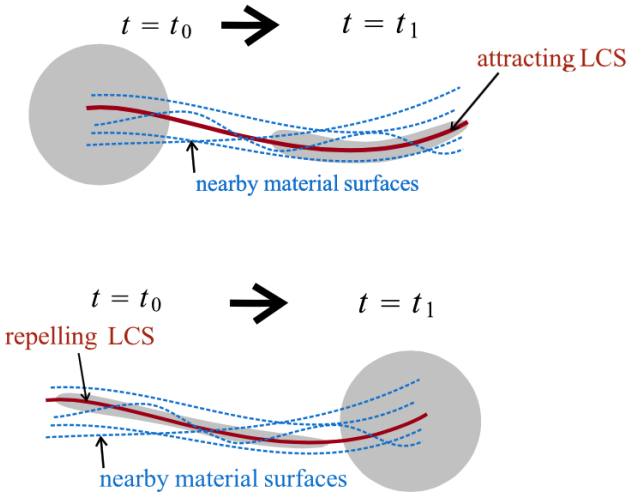

Figure 2.1: Hyperbolic LCS. Capture from [8].

This definition captures the main physical property of a hyperbolic LCS but there is no mathematical definition that allows computing LCS in dynamical systems. Two different mathematical approaches that had been developed until now will be given in this chapter, the first one is related to the *FTLE field* and the second is called *Variational LCS theory*.

Simple counterexamples in [8] reveal conceptual problems in the first theory and thus, the second theory explained below was developed. Despite that, FTLE remain useful as a popular and visual tool to see the global repulsion behavior in complex dynamical systems.

2.2 The finite-time Lyapunov Exponents

In this section, the theory around the Finite-time Lyapunov exponents field and it's correlation with LCS is going to be explained. This theory was developed between 2002 and 2010 in [15, 16, 20].

2.2.1 Definition (Finite-time Lyapunov Exponents field) The field called *Finite-time Lyapunov Exponents (FTLE)* is the field $\sigma_{t_0}^T : D \subseteq \mathbb{R}^n \to \mathbb{R}$ defined by

$$\sigma_{t_0}^T(\mathbf{x}) = \frac{1}{|T|} \ln \sqrt{\lambda_n(\Delta)}$$

where $\lambda_n(\Delta)$ is the largest eigenvalue of the Cauchy-Green Tensor defined in (1.3.4).

For the remainder of this section, in order to avoid degeneracy and non-regularity in the FTLE field, [15, 20], it will be assumed that $0 < \lambda_i < 1$, $i = 1, \cdots, n-1$, and $\lambda_n > 1$. Adding the assumption from Definition 1.1, one can ensure that $\sigma_{t_0}^T(\mathbf{x})$ is C^2 in space and C^1 in time and that LCS are $n-1-$dimensional material surfaces, [20].

Given this field that measures the maximum expansion rate for a pair of near particles by the advection of the flow, the authors of [15] and [20] agreed in describing repelling LCS as the *ridges* of the FTLE field.

In the $2-$dimensional phase space case, it is easy to find the *ridges* of the FTLE field by visual inspection because it's graph is a surface in $\mathbb{R}^3$. So that, one can easily find the repelling LCS by inspection in FTLE plots such the one below:

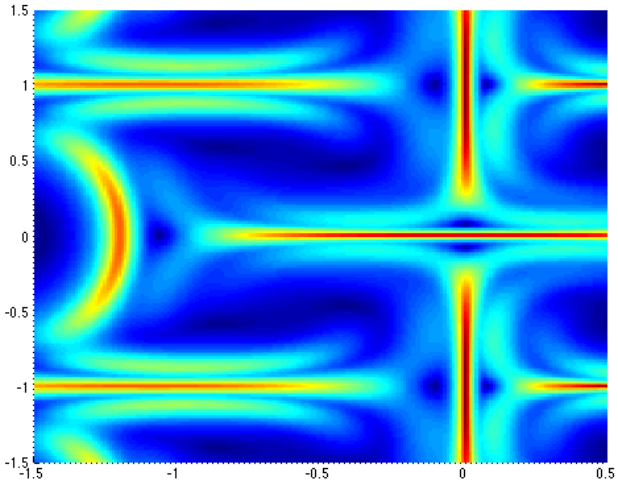

Figure 2.2: Classic FTLE plot for a $2-$dimensional plot. (grid: 200×200)

In Figure 2.2, one can intuit the ridges of the field plotted in red. According to this theory, those ridges plotted in red are the repelling LCS of the Dynamical System over

the interval $[t_0, t_0 + T]$. In that cases, one can parameterize the LCS by interpolation methods of the form $\gamma : (a, b) \to \Omega \subseteq \mathbb{R}^2$ because it is $1-$dimensional. To generalize the idea of LCS as ridges of the FTLE field in $n-$dimensional dynamical systems, one can use the notion of second derivative extrema. So then,

2.2.2 Definition (Repelling LCS) A *repelling LCS* is a codimension 1, orientable and differentiable manifold $\mathcal{M} \subset \Omega \subseteq \mathbb{R}^n$ satisfying the following conditions for each point $\mathbf{x} \in \mathcal{M}$:

1) The unit normal vector $\mathbf{n}(\mathbf{x})$ to the manifold $\mathcal{M}$ is orthogonal to $\nabla \sigma_{t_0}^T(\mathbf{x})$.

2) Let $\Sigma = D_{\mathbf{x}}^2 \sigma_{t_0}^T(\mathbf{x}_0)$ be the Hessian matrix of $\sigma_{t_0}^T(\mathbf{x})$, thought as a bilinear form evaluated at $\mathbf{x}$, we require:
$$\Sigma(\mathbf{n}, \mathbf{n}) < 0$$
and
$$\Sigma(\mathbf{n}, \mathbf{n}) < \Sigma(\mathbf{u}, \mathbf{u})$$
for all unit vectors $\mathbf{u}$ such that $\langle \mathbf{u}, \mathbf{n} \rangle \neq \pm 1$.

Orientation of $\mathcal{M}$ is needed to ensure the uniqueness of the normal vector $\mathbf{n}(\mathbf{x})$.

2.2.3 Definition (Attracting LCS) An *attracting LCS* is a repelling LCS of the backward-time flow, i.e. when integration time goes from $t_0 + T$ to t_0.

As said before, the FTLE field as tool to find hyperbolic LCS presents some inconsistencies in some dynamical systems. In fact, *G. Haller* in [8], subsection 2.3, gave some simple and relevant examples that show that FTLE theory is not good enough.

To summarize the information obtained by these three examples:

1) *Observed LCS are not necessarily ridges of the FTLE field*, as one can notice in the *non-linear saddle flow* system (example 1 in [8]). This shows that the association of LCS to FTLE ridges is not always correct. In the cases of saddle flows, symmetry at the LCS gives wrong results.

2) *Ridges of FTLE field are not necessarily Hyperbolic LCS*. FTLE field presents ridges also to indicate important shearings, which are *parabolic LCS*. In fact, this procedure ignores if the direction $\boldsymbol{\xi}_n$ associated to the largest eigenvalue is close to the tangent direction of $\mathcal{M}(t_0)$, which provokes shearing instead of repelling deformation.

3) *FTLE ridges could break the* 2 *key properties of Proposition 2.1.1.* The properties of *coherence* and *Lagrangian* are important by definition.

In conclusion, the FTLE ridges are an heuristic procedure to find LCS. Hence, one does not have the certainty of the results obtained. However, this procedure is visual and fast, compared to the Variational LCS theory. Therefore, it is essential to know when it is applicable. In general, it can be used as support for quick estimations and preliminary designs.

2.3 The Variational LCS theory

In order to solve the inconsistencies given by the last examples, *G. Haller* presented the mathematical theory that is going to be developed in the next section. This new theory is used to develop the LCS finding algorithms. This section is based on sections 3 and 4 of the article [8] and its correction [4], by *G. Haller* and *M. Farazmand*.

Consider an arbitrary material surface $\mathcal{M}(t) \subset \mathbb{R}^n$. As defined, this manifold is $n-1-$dimensional, hence, at an initial point $\mathbf{x}_0 \in \mathcal{M}(t_0)$, one can consider the tangent space, $T_{\mathbf{x}_0}\mathcal{M}(t_0)$, and the normal space, $\mathbf{n}_0 := N_{\mathbf{x}_0}\mathcal{M}(t_0)$, $n-1-$dimensional and $1-$dimensional respectively. Those two spaces can be advected by the linearized flow map $D_{\mathbf{x}_0}\boldsymbol{\phi}_{t_0}^t(\mathbf{x}_0)$, as shown:

$$\begin{aligned} \mathcal{M}(t_0) &\rightsquigarrow \boldsymbol{\phi}_{t_0}^t(\mathcal{M}(t_0)) \\ T_{\mathbf{x}_0}\mathcal{M}(t_0) &\rightsquigarrow D_{\mathbf{x}_0}\boldsymbol{\phi}_{t_0}^t(\mathbf{x}_0)\ T_{\mathbf{x}_0}\mathcal{M}(t_0) \\ \mathbf{n}_0 &\rightsquigarrow D_{\mathbf{x}_0}\boldsymbol{\phi}_{t_0}^t(\mathbf{x}_0)\ \mathbf{n}_0 \end{aligned}$$

By properties of the linearized flow map, the tangent space is advected to the tangent space of $\mathcal{M}(t)$ at $\mathbf{x}_t = \boldsymbol{\phi}_{t_0}^t(\mathbf{x}_0)$. By contrast, the advected normal vector is generally not coincident to the normal space $\mathbf{n}_t := N_{\mathbf{x}_t}\mathcal{M}(t)$, as can be seen in Figure 2.3.

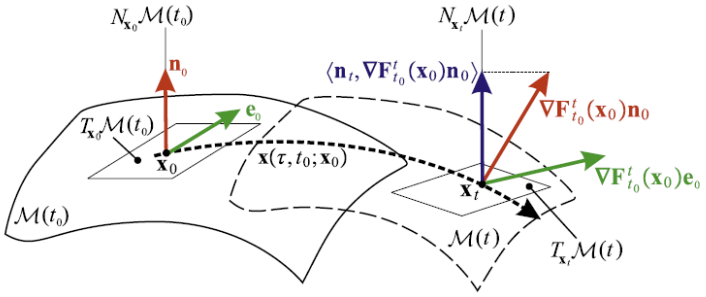

Figure 2.3: Advection of $\mathcal{M}(t_0)$, $T_{\mathbf{x}_0}\mathcal{M}(t_0)$, and $\mathbf{n}_0$. Capture from [8], where $\nabla\mathbf{F}_{t_0}^t(\mathbf{x}_0) \equiv D_{\mathbf{x}_0}\phi_{t_0}^t(\mathbf{x}_0)$.

Thus, $D_{\mathbf{x}_0}\boldsymbol{\phi}_{t_0}^t(\mathbf{x}_0)\ \mathbf{n}_0$ has a general orientation on the space and can be expressed as following:

$$D_{\mathbf{x}_0}\boldsymbol{\phi}_{t_0}^t(\mathbf{x}_0)\ \mathbf{n}_0 = \rho_{t_0}^t(\mathbf{x}_0, \mathbf{n}_0) \cdot \mathbf{n}_t + \pi_{t_0}^t(\mathbf{x}_0, \mathbf{n}_0) \cdot T_{\mathbf{x}_t}\mathcal{M}(t)$$

1 Remark $\pi_{t_0}^t(\mathbf{x}_0, \mathbf{n}_0)$ is the projection of $D_{\mathbf{x}_0}\boldsymbol{\phi}_{t_0}^t(\mathbf{x}_0)\ \mathbf{n}_0$ at $T_{\mathbf{x}_t}\mathcal{M}(t)$ called the *net shear* of $\mathcal{M}(t)$ over a finite-time interval.

2.3.1 Definition (Repulsion rate) The projection of $D_{\mathbf{x}_0}\boldsymbol{\phi}_{t_0}^t(\mathbf{x}_0)\ \mathbf{n}_0$ to the unitary normal space of $\mathcal{M}(t)$ at $\mathbf{x}_t$ is called the *repulsion rate* and it's denoted by $\rho_{t_0}^t(\mathbf{x}_0, \mathbf{n}_0)$:

$$\rho_{t_0}^t(\mathbf{x}_0, \mathbf{n}_0) = \left\langle \mathbf{n}_t, D_{\mathbf{x}_0}\boldsymbol{\phi}_{t_0}^t(\mathbf{x}_0)\ \mathbf{n}_0 \right\rangle$$

The repelling and attracting nature of the surface is captured by this parameter. $\rho_{t_0}^t(\mathbf{x}_0, \mathbf{n}_0) > 1$ indicates that the normal component of normal perturbations to $\mathcal{M}(t_0)$ grows by time. Similarly, when $\rho_{t_0}^t(\mathbf{x}_0, \mathbf{n}_0) < 1$ indicates average attraction at the normal direction.

2.3.2 Definition (Repulsion ratio) The ratio between normal and tangential growth after a finite-interval time is

$$\nu_{t_0}^t(\mathbf{x}_0, \mathbf{n}_0) = \min_{\substack{|\mathbf{e}_0| = 1 \\ \mathbf{e}_0 \in T_{\mathbf{x}_0}\mathcal{M}(t_0)}} \frac{\left\langle \mathbf{n}_t, D_{\mathbf{x}_0}\boldsymbol{\phi}_{t_0}^t(\mathbf{x}_0)\ \mathbf{n}_0 \right\rangle}{\left| D_{\mathbf{x}_0}\boldsymbol{\phi}_{t_0}^t(\mathbf{x}_0)\ \mathbf{e}_0 \right|}$$

Then, $\nu_{t_0}^t(\mathbf{x}_0, \mathbf{n}_0) > 1$ indicates that infinitesimal normal growth along $\mathcal{M}(t)$ dominates the largest tangential growth. In that case, $\mathcal{M}(t)$ is the locally dominant repelling structure at $\mathbf{x}_0$.

The next proposition gives a manner to compute and estimate $\rho_{t_0}^t$ and $\nu_{t_0}^t$ in terms of the Cauchy-Green strain tensor.

2.3.3 Proposition The quantities defined above can be computed and estimated as follows:

1) Computation:

$$\rho_{t_0}^t(\mathbf{x}_0, \mathbf{n}_0) = \frac{1}{\sqrt{\langle \mathbf{n}_0, \Delta^{-1}\ \mathbf{n}_0 \rangle}}$$

$$\nu_{t_0}^t(\mathbf{x}_0, \mathbf{n}_0) = \min_{\substack{|\mathbf{e}_0| = 1 \\ \mathbf{e}_0 \in T_{\mathbf{x}_0}\mathcal{M}(t_0)}} \frac{\rho_{t_0}^t(\mathbf{x}_0, \mathbf{n}_0)}{\sqrt{\langle \mathbf{e}_0, \Delta\ \mathbf{e}_0 \rangle}}$$

where Δ^{-1} stands for the inverse matrix of $\Delta(\mathbf{x}_0, t_0, t)$, i.e. $\Delta^{-1} := \Delta^{-1}(\mathbf{x}_0, t_0, t)$.

2) Estimation:

$$\sqrt{\lambda_1(\mathbf{x}_0, t_0, T)} \leq \rho_{t_0}^{t_0+T}(\mathbf{x}_0, \mathbf{n}_0) \leq \sqrt{\lambda_n(\mathbf{x}_0, t_0, T)}$$

$$\sqrt{\frac{\lambda_1(\mathbf{x}_0, t_0, T)}{\lambda_n(\mathbf{x}_0, t_0, T)}} \leq \nu_{t_0}^{t_0+T}(\mathbf{x}_0, \mathbf{n}_0) \leq \sqrt{\frac{\lambda_n(\mathbf{x}_0, t_0, T)}{\lambda_1(\mathbf{x}_0, t_0, T)}}$$

where λ_1 and λ_n are the lowest and the greatest eigenvalues of $\Delta(\mathbf{x}_0, t_0, T)$.

2 Proof The proof of Proposition 2.3.3 can be found in section 3.1 of [8].

□

Right now, it's possible to define one set of material surfaces, those that are normally repelling or attracting over a time interval. Inside this subset, one can find the most normally repelling or attracting material surfaces, called *Hyperbolic LCS*.

2.3.4 Definition (Normally repelling (attracting) material surface) Given a material surface $\mathcal{M}(t) \subset \Omega$, it is *normally repelling over* $[t_0, t_0 + T]$ if for all points $\mathbf{x}_0 \in \mathcal{M}(t_0)$ and unit normal $\mathbf{n}_0$,

$$\rho_{t_0}^{t_0+T}(\mathbf{x}_0, \mathbf{n}_0) > 1 \ , \quad \nu_{t_0}^{t_0+T}(\mathbf{x}_0, \mathbf{n}_0) > 1$$

are satisfied.

Similarly, $\mathcal{M}(t)$ is *normally attracting over* $[t_0, t_0 + T]$ if it's normally repelling over in backward time. Both of them can be also called *hyperbolic material surface over* $[t_0, t_0 + T]$.

$\rho_{t_0}^{t_0+T}(\mathbf{x}_0, \mathbf{n}_0) > 1$ indicates normal stretches in $\mathbf{x}_0$. $\nu_{t_0}^{t_0+T}(\mathbf{x}_0, \mathbf{n}_0) > 1$ ensures that any tangential deformation along $\mathcal{M}(t)$ is strictly smaller than the repelling force in the normal direction.

2.3.5 Definition (Hyperbolic LCS) A normal repelling (attracting) material surface $\mathcal{M}(t)$ is called a *repelling (attracting) LCS over* $[t_0, t_0+T]$ if its normal repulsion rate admits a pointwise non-degenerate maximum along $\mathcal{M}(t_0)$ among all locally C^1-close material surfaces.

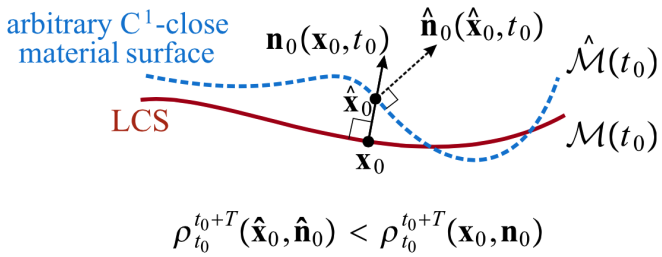

Figure 2.4: LCS definition as an extremum surface for the normal repulsion rate.

2 Remark The mathematical point of view of Definition 2.3.5 is asking to accomplish the non-degenerate relative minimum condition at any point $\mathbf{x}_0 \in \mathcal{M}(t_0)$:

$$\frac{\partial}{\partial \varepsilon} \rho_{t_0}^{t_0+T}(\mathbf{x}_\varepsilon(t_0), \mathbf{n}_\varepsilon(t_0))|_{\varepsilon=0} = 0$$

$$\frac{\partial^2}{\partial \varepsilon^2} \rho_{t_0}^{t_0+T}(\mathbf{x}_\varepsilon(t_0), \mathbf{n}_\varepsilon(t_0))|_{\varepsilon=0} < 0$$

where $\mathbf{x}_\varepsilon(t_0) = \mathbf{x}_0 + \varepsilon\alpha(\mathbf{x}_0, t_0)\mathbf{n}_0(t_0)$ and $\alpha(\mathbf{x}_0, t)$ is an appropiate smooth function.

Choosing an appropiate continuous (with respect to $\mathbf{x}_0$) function $\alpha(\mathbf{x}_0, t_0)$, one constructs all the C^1-close material surfaces.

After defining the concept of *Hyperbolic LCS*, one has to set the sufficient and necessary conditions that ensure the existence of an LCS. [8] gives the most important theorem (Theorem 7) of the Variational LCS theory. Based on that theorem, Theorem 2.3.6 gives a clear relation between LCS and the invariants of the finite-time Cauchy-Green strain tensor.

2.3.6 Theorem (Sufficient and necessary conditions for an LCS) *Given a compact material surface $\mathcal{M}(t) \subset \Omega \subset \mathbb{R}^n$ over the interval $[t_0, t_0+T]$. Then, $\mathcal{M}(t)$ is a repelling LCS over $[t_0, t_0+T]$ if and only if all the following hold for all $\boldsymbol{x}_0 \in \mathcal{M}(t_0)$:*

1) $\lambda_{n-1}(\boldsymbol{x}_0, t_0, T) \neq \lambda_n(\boldsymbol{x}_0, t_0, T) > 1$

2) $\boldsymbol{\xi}_n(\boldsymbol{x}_0, t_0, T) \perp T_{\boldsymbol{x}_0}\mathcal{M}(t_0)$

3) $\langle D_{\boldsymbol{x}_0}\lambda_n(\boldsymbol{x}_0, t_0, T),\ \boldsymbol{\xi}_n(\boldsymbol{x}_0, t_0, T)\rangle = 0$

4) The matrix $\boldsymbol{L}(\boldsymbol{x}_0, t_0, T) \in \mathcal{M}_n(\mathbb{R})$, see Matrix 2.1, is positive definite for all $\boldsymbol{x}_0 \in \mathcal{M}(t_0)$

where λ_i and $\boldsymbol{\xi}_i$ are the eigenvalues and the eigenvectors of $\Delta(\boldsymbol{x}_0, t_0, T)$.

$$\boldsymbol{L}(\boldsymbol{x}_0, t_0, T) = \begin{pmatrix} D^2_{\boldsymbol{x}_0}\Delta^{-1}[\boldsymbol{\xi}_n] & 2\frac{\lambda_n-\lambda_1}{\lambda_1\lambda_n}\langle \boldsymbol{\xi}_1, D_{\boldsymbol{x}_0}\boldsymbol{\xi}_n\boldsymbol{\xi}_n\rangle & \cdots & 2\frac{\lambda_n-\lambda_{n-1}}{\lambda_{n-1}\lambda_n}\langle \boldsymbol{\xi}_{n-1}, D_{\boldsymbol{x}_0}\boldsymbol{\xi}_n\boldsymbol{\xi}_n\rangle \\ 2\frac{\lambda_n-\lambda_1}{\lambda_1\lambda_n}\langle \boldsymbol{\xi}_1, D_{\boldsymbol{x}_0}\boldsymbol{\xi}_n\boldsymbol{\xi}_n\rangle & 2\frac{\lambda_n-\lambda_1}{\lambda_1\lambda_n} & \cdots & 0 \\ \vdots & \vdots & \ddots & \vdots \\ 2\frac{\lambda_n-\lambda_{n-1}}{\lambda_{n-1}\lambda_n}\langle \boldsymbol{\xi}_{n-1}, D_{\boldsymbol{x}_0}\boldsymbol{\xi}_n\boldsymbol{\xi}_n\rangle & 0 & \cdots & 2\frac{\lambda_n-\lambda_{n-1}}{\lambda_{n-1}\lambda_n} \end{pmatrix} \tag{2.1}$$

where the first term is

$$D^2_{\boldsymbol{x}_0}\Delta^{-1}[\boldsymbol{\xi}_n] = -\frac{1}{\lambda_n^2}\left\langle \boldsymbol{\xi}_n, D^2_{\boldsymbol{x}_0}\lambda_n\boldsymbol{\xi}_n\right\rangle + 2\sum_{q=1}^{n-1}\frac{\lambda_n-\lambda_q}{\lambda_n\lambda_q}\langle \boldsymbol{\xi}_q, D_{\boldsymbol{x}_0}\boldsymbol{\xi}_n\boldsymbol{\xi}_n\rangle^2$$

3 Remark Matrix $\mathbf{L}(\mathbf{x}_0, t_0, T)$ comes from the proof of the theorem. It has no explicit meaning, it's just a way to put some inequalities in order using Sylvester criteria for positive definiteness. Moreover, future developments will show that matrix $\mathbf{L}(\mathbf{x}_0, t_0, T)$ will be never computed in $2-$dimensional systems, another equivalent condition will be established in proposition 2.3.7.

3 Proof A scheme of the proof is shown below. This proof was made by *G.Haller*'s group in [8]. Further details and the complete proof can be found in [8], section 4.1, with some corrections in Erratum [4].

1st step Prove that condition (1), (2) and (3) are necessary:

The extremum property of the repulsion rate along $\mathcal{M}(t)$ is going to be formulated. For that, a C^1-material surface nearby $\mathcal{M}(t)$, $\mathcal{M}_\varepsilon(t)$ is constructed by the same development used in remark 2, points $\mathbf{x}_\varepsilon(t_0) \in \mathcal{M}_\varepsilon(t)$ are of the form:

$$\mathbf{x}_\varepsilon(t_0) = \mathbf{x}_0 + \varepsilon\alpha(\mathbf{x}_0, t_0)\mathbf{n}_0(t_0)$$

with an appropiate smooth function $\alpha : \Omega \times I \to \Omega$.

Imposing,

$$\frac{\partial}{\partial\varepsilon}\rho_{t_0}^{t_0+T}(\mathbf{x}_\varepsilon(t_0), \mathbf{n}_\varepsilon(t_0))|_{\varepsilon=0} = 0 \tag{2.2}$$

some developments that are shown by detail in [8], using Proposition 2.3.3 and Taylor developments of $\mathbf{n}_\varepsilon(t_0)$ around $\mathbf{n}_0$, one arrives to

$$\sum_{i,j=1}^{n}\sum_{p=1}^{n-1}\Delta^{-1}_{ij}(\mathbf{x}_0)e^i_p n^j_0 = 0 \tag{2.3}$$

$$\sum_{i,j,k=1}^{n}\Delta^{-1}_{ij,k}(\mathbf{x}_0)\xi^i_n\xi^j_n\xi^k_n = 0 \tag{2.4}$$

where $\Delta^{-1}_{ij,k}$ is the differentation of Δ^{-1}_{ij} with respect to x^k, $\mathbf{u}^i$ is the $i-$th component of the vector $\mathbf{u}$ and $\mathbf{e}_p$, $p = 1, \cdots, n-1$ form an orthonormal basis of $T_{\mathbf{x}_0}\mathcal{M}(t_0)$.

By differentiating the eigenvalue problem of Δ^{-1} with respect to x^k, and using the identity $\sum_{i=1}^{n}\xi^i_n\xi^i_n = 1$ and its differentation, one obtains:

$$\sum_{i,j=1}^{n}\Delta^{-1}_{ij,k}\xi^i_n\xi^j_n = -\frac{\lambda_{n,k}}{\lambda^2_n}$$

which implies, using equation (2.4),

$$\langle D_{\mathbf{x}_0}\lambda_n, \boldsymbol{\xi}_n\rangle = \sum_{k=1}^{n}\lambda_{n,k}\xi^k_n = -\lambda^2_n\sum_{i,j,k=1}^{n}\Delta^{-1}_{ij,k}(\mathbf{x}_0)\xi^i_n\xi^j_n\xi^k_n = 0$$

so then, condition (3) of the theorem is necessary.

Note that equation (2.3) implies directly $\Delta^{-1}\mathbf{n}_0 \perp T_{\mathbf{x}_0}\mathcal{M}(t_0)$, which is condition (2). Equivalently, $\Delta^{-1}\mathbf{n}_0 || \mathbf{n}_0$, which states that $\mathbf{n}_0$ must be an eigenvector of Δ^{-1}. Definition 2.3.4 forces $\mathbf{n}_0$ to be $\boldsymbol{\xi}_n$ and the corresponding eigenvalue λ_n to be multiplicity one, which makes condition (1) necessary (adding that $\nu^t_{t_0} > 1$).

2nd step Prove that condition (4) is necessary:

To prove condition (4), one has to ensure to have a non-degenerate local maximum of $\rho^t_{t_0}$ in $\mathbf{n}_0$ direction, so then

$$\frac{\partial^2}{\partial\varepsilon^2}\rho^{t_0+T}_{t_0}(\mathbf{x}_\varepsilon(t_0), \mathbf{n}_\varepsilon(t_0))|_{\varepsilon=0} < 0 \tag{2.5}$$

Procedures similar to those on step 1, that can be found in [8], prove that (4) is needed to be an LCS.

3rd step Conditions are also sufficient:

Applying $\boldsymbol{\xi}_n \equiv \mathbf{n}_0$, result obtained in 1st step, in Proposition 2.3.3, one deduces:

$$\rho^{t_0+T}_{t_0} = \sqrt{\lambda_n} > 1$$

$$\nu^{t_0+T}_{t_0} = \sqrt{\frac{\lambda_n}{\lambda_{n-1}}} > 1$$

That results holding for all $\mathbf{x}_0 \in \mathcal{M}(t_0)$ implies that $\mathcal{M}(t_0)$ is a normally repelling material surface. Furthermore, we have seen that (1), (2) and (3) derive from Equation 2.2 and proved the sufficiency of that conditions. Finally, the positive definiteness of $\mathbf{L}(\mathbf{x}_0, t_0, T)$ guarantees that Equation 2.5 is satisfied. Hence, the four conditions are also sufficient.

□

4 Remark In the 3rd step of the proof, new ways to compute $\rho_{t_0}^{t_0+T}$ and $\nu_{t_0}^{t_0+T}$ have been found when $\mathcal{M}(t)$ is an LCS. The new value of $\rho_{t_0}^{t_0+T} = \sqrt{\lambda_n(\mathbf{x}_0, t_0, T)}$ is the maximal value that it can take because of the Estimation given in Proposition 2.3.3.

Next chapter is dedicated to the computation of LCS in continuous 2−dimensional dynamical systems. Therefore, Theorem 2.3.6 in 2−dimensional dynamical systems can be re-written as follows, in order to avoid to compute the matrix $\mathbf{L}(\mathbf{x}_0, t_0, T)$.

2.3.7 Proposition (Sufficient and necessary conditions for Hyperbolic LCS) Given a compact material surface $\mathcal{M}(t) \subset \Omega \in \mathbb{R}^2$ which is a *repelling LCS* over the interval $[t_0, t_0 + T]$. Then:

1) $\lambda_1(\mathbf{x}_0, t_0, T) \neq \lambda_2(\mathbf{x}_0, t_0, T) > 1$

2) $\left\langle \boldsymbol{\xi}_2(\mathbf{x}_0, t_0, T), D^2_{\mathbf{x}_0}\lambda_2(\mathbf{x}_0, t_0, T)\xi_2(\mathbf{x}_0, t_0, T) \right\rangle < 0$

3) $\boldsymbol{\xi}_2(\mathbf{x}_0, t_0, T) \perp T_{\mathbf{x}_0}\mathcal{M}(t_0)$

4) $\langle \boldsymbol{\xi}_2(\mathbf{x}_0, t_0, T),\ D_{\mathbf{x}_0}\lambda_2(\mathbf{x}_0, t_0, T) \rangle = 0$

4 Proof Conditions (1), (3) and (4) came directly from theorem 2.3.6. Condition (2) derives from the application of Sylvester's criteria to the matrix $\mathbf{L}(\mathbf{x}_0, t_0, T)$, which asks to the leading principal minors of $\mathbf{L}$ to be positive, so then:

$$D^2_{\mathbf{x}_0}\Delta^{-1}[\boldsymbol{\xi}_n] = -\frac{1}{\lambda_2^2}\left\langle \boldsymbol{\xi}_2, D^2_{\mathbf{x}_0}\lambda_2\boldsymbol{\xi}_2 \right\rangle + 2\frac{\lambda_2 - \lambda_1}{\lambda_1\lambda_2}\left\langle \boldsymbol{\xi}_1, D_{\mathbf{x}_0}\boldsymbol{\xi}_2\boldsymbol{\xi}_2 \right\rangle^2 > 0 \tag{2.6}$$

$$\det \mathbf{L} = 2\frac{\lambda_2 - \lambda_1}{\lambda_1\lambda_2}D^2_{\mathbf{x}_0}\Delta^{-1}[\boldsymbol{\xi}_n] - \left(2\frac{\lambda_2 - \lambda_1}{\lambda_1\lambda_2}\right)^2 \left\langle \boldsymbol{\xi}_1, D_{\mathbf{x}_0}\boldsymbol{\xi}_2\boldsymbol{\xi}_2 \right\rangle > 0 \tag{2.7}$$

From inequality 2.6 one derives to

$$\left\langle \boldsymbol{\xi}_1, D_{\mathbf{x}_0}\boldsymbol{\xi}_2\boldsymbol{\xi}_2 \right\rangle^2 > \frac{\lambda_1}{2\lambda_2(\lambda_2 - \lambda_1)}\left\langle \boldsymbol{\xi}_2, D^2_{\mathbf{x}_0}\lambda_2\boldsymbol{\xi}_2 \right\rangle \tag{2.8}$$

and from inequality 2.7

$$-2\frac{\lambda_2 - \lambda_1}{\lambda_1\lambda_2^3}\left\langle \boldsymbol{\xi}_2, D^2_{\mathbf{x}_0}\lambda_2\boldsymbol{\xi}_2 \right\rangle > 0 \tag{2.9}$$

Inequality 2.9 is equivalent to $\left\langle \boldsymbol{\xi}_2, D^2_{\mathbf{x}_0}\lambda_2\boldsymbol{\xi}_2 \right\rangle < 0$ because $\lambda_2 > \lambda_1 > 0$. Finally, using this last inequality in 2.8, one arrives to condition 2, as desired.

□

Proposition 2.3.7 will be used to define new objects and properties that will be useful to construct an algorithm to do it computationally.

3
Computation of LCS

This chapter is dedicated to the computation methods to find LCS in 2−dimensional Dynamical Systems, so then, $n = 2$ in all the chapter. Furthermore, the assumption of $\lambda_{n-1} < 1 < \lambda_n$ applies also in this chapter, so that, $\lambda_1 < 1 < \lambda_2$. In this section, only algorithms for the Repelling LCS are designed. One final section in this chapter gives some analogous results to Attracting LCS.

Algorithms to find the LCS by the two different methods studied are given, firstly the FTLE visualization algorithm, based on [20], and secondly the Variational Theory, [5].

As mentioned, the first theory is not conclusive and will be used only to see the patterns. Second theory will be used to develop an LCS-finder algorithm given any $2D-$Dynamical System

The content of this chapter will be applied in one typical example in non-linear dynamics, *the Double Gyre*. This system was chosen in order to compare all the results obtained with the results shown in [5] which influenced the algorithmics of this thesis.

3.1 Computation of FTLE fields

This section is dedicated to the computation of the finite-time Lyapunov exponents field (FTLE). The first step is to calculate the Cauchy-Green tensor and its eigenvalues $\lambda_1 < 1 < \lambda_2$ and the associated eigenvectors $\boldsymbol{\xi}_1, \boldsymbol{\xi}_2$. For the remainder of this chapter, the nomenclature $\mathcal{E} = \{\lambda_1, \lambda_2, \boldsymbol{\xi}_1, \boldsymbol{\xi}_2\}$ will be used to call the quartet of eigenvalues and eigenvectors of Δ, the Cauchy-Green strain tensor.

Given a Dynamical System of the form of Equation 1.1, let $\mathbf{x}_0 \in \Omega \subseteq \mathbb{R}^2$ be an arbitrary point and let $[t_0, t_0 + T] \subset [\alpha, \beta]$ be the finite-time interval of integration, by Runge-Kutta methods, one can integrate the *Variational Equations*:

$$\begin{cases} \dot{\mathbf{x}}(t) & = & \mathbf{f}(\mathbf{x}(t), t) \\ \mathbf{x}(t_0) & = & \mathbf{x}_0 \\ \dot{\Phi} & = & \mathbf{A}(\mathbf{x}, t)\ \Phi \\ \Phi(t_0; t_0, \mathbf{x}_0) & = & \mathbf{Id}_n \\ \mathbf{x}(t) & \in & \Omega \subseteq \mathbb{R}^2 \\ t & \in & I = [\alpha, \beta] \end{cases} \tag{3.1}$$

in order to find the Jacobian of the flow, $\Phi := \Phi(t_0 + T; t_0, \mathbf{x}_0)$.

5 Remark The Jacobian of the flow, Φ, after a finite-time interval can also be computed by central finite differences, taken from section 4.1 in [19]. Partial derivatives of a function can be approximated by:

$$\frac{\partial f_i}{\partial x_j} \approx \frac{f_i(\mathbf{x} + h\mathbf{e}_j) - f_i(\mathbf{x} - h\mathbf{e}_j)}{2h}$$

By this method, one has to integrate $4n = 4 \cdot 2 = 8$ Ordinary Differential Equations (ODEs). On the other hand, using the Variational Equations given in 3.1 one has to integrate one system of $n + n^2 = 2 + 2^2 = 6$ ODEs.

Note that these ODEs are different to the ones of the other method. Therefore, it is not assured that the Variational Equations are more efficient than central finite differences.

Once Φ is obtained, the Cauchy-Green strain tensor is calculated by $\Delta := \Delta(t_0 + T; t_0, \mathbf{x}_0) = \Phi^T \cdot \Phi$ and its quartet $\mathcal{E}$ is computed with an eigenvalue problem solver.

The FTLE field requires the value of the greatest eigenvalue λ_2, as shown in Definition 2.2.1. Once λ_2 is calculated, one can easily compute the FTLE field.

The algorithm to compute the FTLE graphics is the following:

Algorithm 1 FTLE visualization algorithm

```
% G_0 ⊂ Ω is the grid of initial conditions in the phase space.
% [t_0, t_0 + T] is the interval of integration.
while x_0 ∈ G_0 do
  Obtaining Φ by integration of the System 3.1
  Δ := Φ^T · Φ
  Obtaining E = {λ_1, λ_2, ξ_1, ξ_2} by an eigenvalue solver.
  σ_{t_0}^{t_0+T}(x_0) := 1/|T| ln √(λ_2(Δ))
Plot σ_{t_0}^{t_0+T}(x_0),   ∀x_0 ∈ G_0.
```

3.1.1 Example (The Double Gyre) The Double Gyre is a 2−dimensional non-linear dynamical system given by the equations:

$$\begin{cases} \dot{x} &= -A\pi \sin(\pi f(x,t)) \cos(\pi y) \\ \dot{y} &= A\pi \cos(\pi f(x,t)) \sin(\pi y) \dfrac{\partial f}{\partial x}(x,t) \end{cases} \tag{3.2}$$

where

$$f(x,t) = a(t)x^2 + b(t)x$$

$$a(t) = \varepsilon \sin(\omega t) \quad , \quad b(t) = 1 - 2\ a(t)$$

and A, ε, ω arbitrary parameters. The phase space is $\Omega = [0,2] \times [0,1]$ and the time interval $I = [0, \infty)$. In this computation, the parameters used are $A = 0.1$, $\varepsilon = 0.1$, $\omega = 2\pi/10$, $t_0 = 0$ and $T = 20$, the same values in [5] in order to compare the results obtained with those in this article.

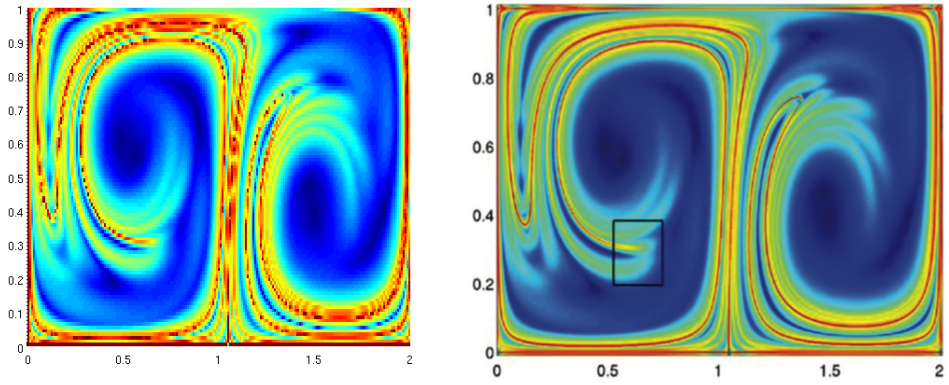

(a) Obtained numerically. (grid: 200×100) (b) Taken from [5].

Figure 3.1: FTLE plots of the Double Gyre.

Figure 3.1a shows the forward-time FTLE plot of the Double Gyre. This plot was obtained numerically with Algorithm 1. Red corresponds to the highest values of the FTLE field. Analogously, blue corresponds to the lowest values. Thus, one can easily detect the ridges of the FTLE field, in red. Recalling Definition 2.2.2, they are the repelling LCS of the system.

As explained in section 2.2, this plot shows an idea of the dynamics of the system but not always the ridges correspond to the repelling LCS. Despite that, the computation is very easy and fast so the computation of this plot gives a preliminary idea of the most repelling areas in the phase space over $[t_0, t_0 + T]$. Further information will be obtained with the implementation of the Variational theory, shown in next section.

3.2 LCS-finder inspired by the Variational theory

The algorithms of this section follow the ideas given in [5]. The intention in this section is to create an LCS-finder from the Variational LCS theory as explained in the cited article.

Remembering Proposition 2.3.7, which gives the sufficient conditions to a material surface for being an LCS, it is necessary to state an efficient algorithm to find the LCS of the phase space.

One should remark the difficulty of computing the 4 statements of Proposition 2.3.7 due to their numerical sensitivity. Computing the quartet $\mathcal{E}$ implies ODE solvers, numerical differentation and eigenvalue problem solvers. After that, one has to compute more derivatives in order to verify the 4 necessary conditions. As given in [5] in section II.B, Proposition 2.3.7 can be reformulated as given below so as to have a more robust implementation:

3.2.1 Proposition (Relaxed Proposition 2.3.7) Given a curve $\Gamma(t_0) \subset \Omega \subset \mathbb{R}^2$ which is a *repelling LCS* over the interval $[t_0, t_0 + T]$. Then, for all points $\mathbf{x}_0 \in \Gamma(t_0)$:

(A) $\lambda_1(\mathbf{x}_0, t_0, T) \neq \lambda_2(\mathbf{x}_0, t_0, T) > 1$

(B) $\left\langle \boldsymbol{\xi}_2(\mathbf{x}_0, t_0, T), D^2_{\mathbf{x}_0}\lambda_2(\mathbf{x}_0, t_0, T)\boldsymbol{\xi}_2(\mathbf{x}_0, t_0, T)\right\rangle < 0$

(C) $\boldsymbol{\xi}_1(\mathbf{x}_0, t_0, T) \mid\mid T_{\mathbf{x}_0}\Gamma(t_0)$

(D) $\bar{\lambda}_2(\Gamma(t_0))$, the average of λ_2 over the curve, is maximal among all nearby curves $\gamma(t_0)$ such that $\gamma(t_0) \mid\mid \boldsymbol{\xi}_1(\mathbf{x}_0, t_0, T)$.

6 Remark Note that in 2−dimensional phase spaces, $T_{\mathbf{x}_0}\Gamma(t_0)$ is 1−dimensional and it is spanned by the tangent vector of the curve $\Gamma(t_0)$ at the point $\mathbf{x}_0 \in \Gamma(t_0)$.

5 Proof Comparing those two Propositions (2.3.7 and 3.2.1), one can notice that first and second conditions did not change.

Condition (3) has been changed to (C) using the orthogonality of $\boldsymbol{\xi}_1$ and $\boldsymbol{\xi}_2$ due to the spectral theorem of linear algebra and using also that $T_{\mathbf{x}_0}\Gamma(t_0)$ is the tangent vector of the curve $\Gamma(t_0)$, see Remark 6.

Condition (4) has been relaxed using the fact that $\mathbf{n}_0 = \boldsymbol{\xi}_2(\mathbf{x}_0, t_0, T)$ and $\rho_{t_0}^{t_0+T} = \sqrt{\lambda_2(\mathbf{x}_0, t_0, T)} > 1$ if $\mathbf{x}_0 \in$ LCS, results taken from the proof of the Theorem 2.3.6, and:

$$\frac{\mathrm{d}}{\mathrm{d}\varepsilon}\rho_{t_0}^{t_0+T}(\mathbf{x}_0 + \varepsilon\boldsymbol{\xi}_2, \boldsymbol{\xi}_2)|_{\varepsilon=0} = \frac{1}{2\sqrt{\lambda_2(\mathbf{x}_0, t_0, T)}}\left\langle \boldsymbol{\xi}_2(\mathbf{x}_0, t_0, T),\ D_{\mathbf{x}_0}\lambda_2(\mathbf{x}_0, t_0, T)\right\rangle = 0$$

This result says that the repulsion rate is a maximum on $\boldsymbol{\xi}_2$ direction for all nearby curves. That allows to relax condition (4), of Proposition 2.3.7, to condition (D), of Proposition 3.2.1.

□

The design of the final algorithm to find LCS uses Proposition 3.2.1. Sufficient conditions to be a repelling LCS are given and the key is to find a manner to compute all of them efficiently. For this reason, next sections give some results and ideas that will approach us to the final Algorithm 3.

3.2.1 The strainlines

From condition (C) of Proposition 3.2.1, one can notice that the LCS are those curves, $\Gamma(t_0)$, tangent to $\boldsymbol{\xi_1}$, the eigenvector associated to the smallest eigenvalue, λ_1, $\forall \mathbf{x}_0 \in \Gamma(t_0)$. So then, there's a new set of curves in the phase space:

3.2.2 Definition (Strainline) Given a Dynamical System of the form 1.1 and a finite-time interval $I = [t_0, t_0 + T]$. A *strainline* is a curve $\gamma(t_0) \subset \Omega$ such that it is the orbit of the Cauchy problem:

$$\left\{\begin{array}{rcl} \mathbf{x}'(s) & = & \boldsymbol{\xi}_1(\mathbf{x}(s), t_0, T) \\ \mathbf{x}(0) & = & \mathbf{x}_0 \in \Omega \\ |\boldsymbol{\xi}_1| & = & 1 \end{array}\right. \tag{3.3}$$

where $\boldsymbol{\xi}_1 = \boldsymbol{\xi}_1(\mathbf{x}(s), t_0, T)$ stands for the smallest eigenvector calculated at $\mathbf{x} \in \Omega$ integrating from t_0 to $t_0 + T$.

Hence, the LCS set is the subset of the strainlines that satisfies conditions (A), (B) and (D) of Proposition 3.2.1.

In order to be more efficient numerically, an appropiate scaling in the velocity map of System 3.5, suggested in [5], is presented:

$$\begin{cases} \mathbf{x}'(s) &= \tilde{\boldsymbol{\xi}}_1(\mathbf{x}(s), t_0, T) \\ \mathbf{x}(0) &= \mathbf{x}_0 \in \Omega \end{cases} \tag{3.4}$$

where $\tilde{\boldsymbol{\xi}}_1(\mathbf{x}(s), t_0, T) = \text{sign}(\mathbf{x}(s))\alpha(\mathbf{x}(s))\boldsymbol{\xi}_1(\mathbf{x}(s), t_0, T)$ is the product of these 3 maps:

- $\boldsymbol{\xi}_1(\mathbf{x}(s), t_0, T)$ is the eigenvector of the Cauchy-Green strain tensor computed as in Algorithm 1.
- Function $\alpha(\mathbf{x}(s))$ is needed to stop the solver when approaching possible degenerate points. It is computed as follows:

  $$\alpha(\mathbf{x}(s)) = \left(\frac{\lambda_2(\mathbf{x}(s)) - \lambda_1(\mathbf{x}(s))}{\lambda_2(\mathbf{x}(s)) + \lambda_1(\mathbf{x}(s))}\right)^2$$

  where $\lambda_i(\mathbf{x}(s))$ are the eigenvalues of the Cauchy-Green strain tensor, that are computed as in Algorithm 1.
- $\text{sign}(\mathbf{x}(s))$ ensures the smoothness of the trajectory. Given the tangent vector of $\gamma(t_0)$ at $\mathbf{x}(s)$, if $\mathbf{u}$ is parallel to $\gamma'(t_0)$, then $-\mathbf{u}$ is also parallel to $\gamma'(t_0)$. At each step of the integration, $\mathbf{x}_k$, this function takes the sign of the following inner product $\langle \boldsymbol{\xi}_1(\mathbf{x}_k, t_0, T), \mathbf{x}_{k-1} - \mathbf{x}_k \rangle$. Hence, it ensures that the right eigenvector is chosen to guarantee the smoothness of the curve:

  $$\langle \boldsymbol{\xi}_1(\mathbf{x}_k, t_0, T), \boldsymbol{\xi}_1(\mathbf{x}_{k-1}, t_0, T) \rangle \geq 0$$

As one can notice right now, computing a strainline is also expensive computationally because, for each evaluation of the right-hand side of 3.4, the ODE of the Dynamical System has to be solved from t_0 to $t_0 + T$ in order to obtain the quartet $\mathcal{E}$.

7 Remark Function $\alpha(\mathbf{x}(s))$ ensures also that Condition (A) is satisfied because it stops the solver in the case that there's a degenerate point.

8 Remark As suggested in [5], small LCS have negligible effect on the phase space evolution. To filter out that curves, one parameter is created as a minimum length allowed to be a strainline. This parameter is $l_{\min}$.

3.2.3 Example (The Double Gyre) Using the same example than before, Example 3.1.1, the strainlines are computed, as trajectories of the Cauchy Problem 3.4, and shown in Figure 3.2a. Recalling Remark 8, $l_{\min} = 1$, as in [5].

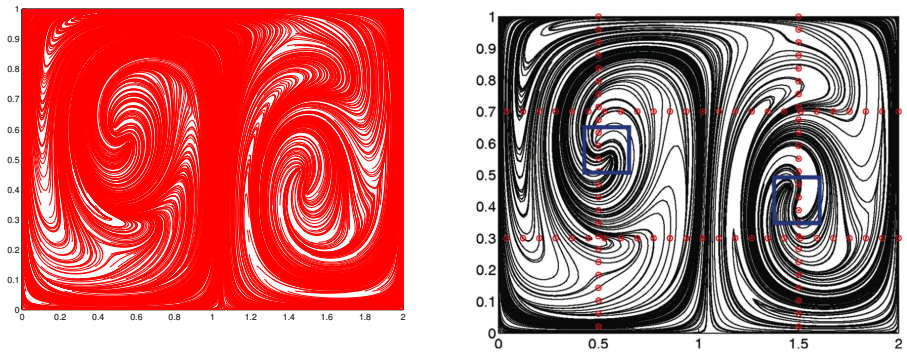

(a) Obtained numerically. (grid: 50×25) (b) Taken from [5].

Figure 3.2: Strainlines of the Double Gyre.

Subfigures from Figure 3.2 show the strainlines of the Double Gyre. On the left, Figure 3.2a, there is the graph obtained computationally with Algorithm 3, using an ODE solver to integrate equations 3.4. On the right, Figure 3.2b, is a capture from the example followed in [5]. Even though the number of strainlines is different, one can see the similarity of the plots.

Those strainlines from Figure 3.2a that satisfy Conditions (B) and (D) of Proposition 3.2.1 will be repelling LCS. To find the LCS, the grid used will be 8 times thiner, 200×50.

3.2.2 The region $\mathcal{U}_0$

3.2.4 Definition (Region $\mathcal{U}_0$) Given a Dynamical System of the form 1.1 and a finite-time interval $I = [t_0, t_0 + T]$. The *region* $\mathcal{U}_0 \subseteq \Omega$ is the region where Condition (B) of Proposition 3.2.1 is satisfied, so then:

$$\mathcal{U}_0 = \left\{\mathbf{x}_0 \in \Omega : \left\langle \boldsymbol{\xi}_2(\mathbf{x}_0, t_0, T), D^2_{\mathbf{x}_0}\lambda_2(\mathbf{x}_0, t_0, T)\boldsymbol{\xi}_2(\mathbf{x}_0, t_0, T)\right\rangle < 0\right\}$$

where $\boldsymbol{\xi}_2(\mathbf{x}_0, t_0, T)$ is the eigenvector associated to the largest eigenvalue $\lambda_2(\mathbf{x}_0, t_0, T)$ and $D^2_{\mathbf{x}_0}\lambda_2(\mathbf{x}_0, t_0, T)$ is the Hessian of the field $\lambda_2(\mathbf{x}_0, t_0, T)$.

Computing region $\mathcal{U}_0$ is expensive computationally and extremely sensitive. For each point $\mathbf{x}_0 \in \mathcal{G}_0$, the trajectory from t_0 to $t_0 + T$ has to be calculated in order to obtain $\mathcal{E} = \{\lambda_1, \lambda_2, \boldsymbol{\xi}_1, \boldsymbol{\xi}_2\}$. After that, the Hessian must be computed. And finally, one should compute the inner product.

9 Remark The Hessian can be computed by double finite differences, see Remark 5, or by other more complex methods. The accuracy of the region $\mathcal{U}_0$ depends on the method used.

In this thesis, a MATLAB code, extracted from [1], is used. This code is in *File Exchange Matlab* website, which works as a sharing-codes place. It is made by John D'Errico, who is in the *Top 10 Authors* of that website with 55 codes and more than 8000 downloads.

Even though double finite differences to compute the Hessian was the fastest procedure, it was discarded because of its low accuracy.

As seen in Figures 3.4, region $\mathcal{U}_0$ is very sensitive to the procedure used to compute the Hessian of $\lambda_2(\mathbf{x}_0, t_0, T)$ and to the grid used. The grid size and the tolerance of the ODE solver are two elements that must be well-adjusted in order to reduce the computation time without losing accuracy.

10 Remark Recalling Proposition 3.2.1, condition (B) must be fulfilled for all the points of an strainline in order to be an LCS candidate. For that reason, Algorithm 3 considers only points $\mathbf{x}_0 \in \mathcal{U}_0$ as initial condition for the strainlines.

While computing the strainline, the inner product must be negative for all points $\mathbf{x}_k$ of the ODE solver. In order to make faster the LCS-finder algorithm, double linear interpolation is used.

Let $\mathbf{x}_k \in \Omega$ be a point of a strainline obtained by using an ODE solver. Then, $\mathbf{x}_k$ is framed by 4 points of the grid, as seen in Figure 3.3. The inner product of condition (B) is calculated by double linear interpolation with the points of the grid with the formula that follows:

$$f(\mathbf{x}_k) \approx \frac{1}{(x_2 - x_1)(y_2 - y_1)}[f(x_1, y_1)(x_2 - x)(y_2 - y) + f(x_2, y_1)(x - x_1)(y_2 - y) + \\ + f(x_1, y_2)(x_2 - x)(y - y_1) + f(x_2, y_2)(x - x_1)(y - y_1)]$$

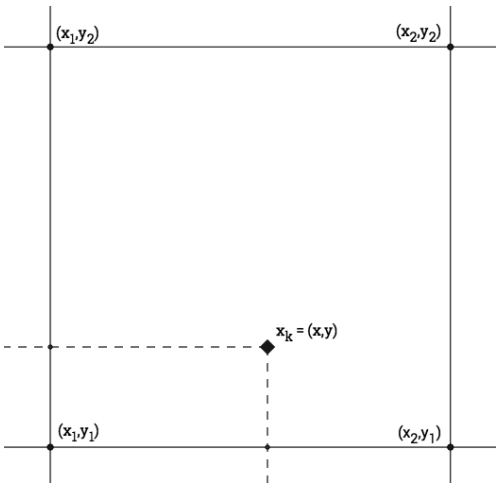

Figure 3.3: Double Linear Interpolation.

11 Remark As suggested in [5], in order to avoid accidentally failures due to numerical errors computing the inner product of condition (B), another filter parameter is used. This parameter is l_f and it is the maximum length of a part of the curve where computed condition (B) is not satisfied. It will be always less than a 20% of the other filter parameter $l_{\min}$ from Remark 8.

3.2.5 Definition (LCS candidate) For the remainder, a strainline that satisfies condition (B), with the filter parameter of Remark 11, is called an *LCS candidate*. If an *LCS candidate* satisfies also condition (D), then it is an LCS.

3.2.6 Example (The Double Gyre) Using the same example than before, Example 3.1.1, with the filter parameter $l_f = 0.2$. The region $\mathcal{U}_0$ is computed as explained in this subsection.

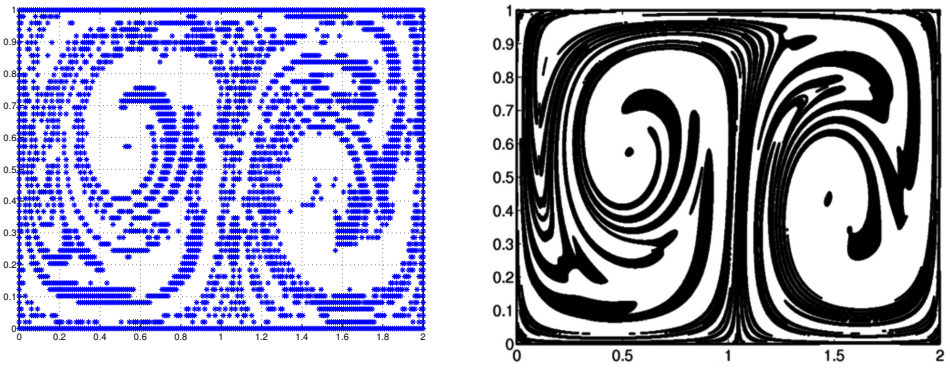

(a) Obtained numerically. (grid: 200×50) (b) Taken from [5].

Figure 3.4: Region $\mathcal{U}_0$ of the Double Gyre.

Subfigures from Figure 3.4 show the region $\mathcal{U}_0$ of the Double Gyre. On the left, Figure 3.4a, there is the graph obtained computationally. On the right, Figure 3.4b, is a caption from the example in [5]. As can be seen in Figure 3.4, the accuracy of the computation affects to the region $\mathcal{U}_0$, the graph obtained from [5] is made with a grid of 1000×500.

3.2.3 LCS candidate $\rightsquigarrow$ LCS

Let $\Gamma(t_0) = \{\mathbf{x}_0, \cdots, \mathbf{x}_{\text{final}}\}$ be an LCS candidate computed using an ODE solver, condition (D) from Proposition 3.2.1 states:

> "$\bar{\lambda}_2(\Gamma(t_0))$, the average of λ_2 over the curve, is maximal among all nearby curves $\gamma(t_0)$ such that $\gamma(t_0) \;||\; \boldsymbol{\xi}_1(\mathbf{x}_0, t_0, T)$."

The algorithm designed to check condition (D) uses the fact that the quartet $\mathcal{E}$ was necessarily computed for all the points of the LCS candidates, $\mathbf{x}_k$. Then, given a step parameter $\varepsilon > 0$, two parallel curves are created as follows:

$$\gamma^+(t_0) := \{\mathbf{x}_0^+, \cdots, \mathbf{x}_{\text{final}}^+\}, \quad \text{where } \mathbf{x}_i^+ = \mathbf{x}_i + \varepsilon\boldsymbol{\xi}_2$$

$$\gamma^-(t_0) := \{\mathbf{x}_0^-, \cdots, \mathbf{x}_{\text{final}}^-\}, \quad \text{where } \mathbf{x}_i^- = \mathbf{x}_i - \varepsilon\boldsymbol{\xi}_2$$

where $i = 0, \ldots,$ final, remembering that $\boldsymbol{\xi}_1 \perp \boldsymbol{\xi}_2$.

Then, the average values of λ_2 field over the three curves, $\Gamma, \gamma^+, \gamma^-$, are calculated by

$$\Lambda_2(\gamma) \approx \frac{\sum_{i=1}^{i=\text{final}} \lambda_2(\mathbf{x}_i) \cdot \|\mathbf{x}_{i-1} - \mathbf{x}_i\|}{\sum_{i=1}^{i=\text{final}} \|\mathbf{x}_{i-1} - \mathbf{x}_i\|}$$

which is a simple numerical aproximation, [19], for the average of the field over the curve:

$$\Lambda_2(\gamma) = \frac{\int_\gamma \lambda_2 \, \mathrm{d}\gamma}{\int_\gamma 1 \, \mathrm{d}\gamma}$$

Once the average quantities are calculated, an LCS candidate becomes an LCS if $\Lambda(\Gamma(t_0))$ is the maximum. This subsection is summarized in Algorithm 2.

Algorithm 2 LCS candidate $\rightsquigarrow$ LCS

% $\Gamma(t_0) \in \mathcal{U}_0 \subset \Omega \subseteq \mathbb{R}^2$ is a strainline that satisfies condition (B).
% $[t_0, t_0 + T]$ is the interval of integration.
% $\Gamma(t_0) = \{\mathbf{x}_0, \cdots, \mathbf{x}_{\text{final}}\}$. It is a set of points because it is computed numerically.
% $\text{length}(\gamma) := \sum_{i=1}^{i=\text{final}} \|\mathbf{x}_{i-1} - \mathbf{x}_i\|$ computes the length of the curve γ.
% $\text{int}(\lambda_2(\gamma(t_0))) := \sum_{i=1}^{i=\text{final}} \lambda_2(\mathbf{x}_i) \cdot \|\mathbf{x}_{i-1} - \mathbf{x}_i\|$ computes the integral of λ_2 field
% over the curve γ.
% ε is a step parameter, as small as desired.
while $i = 0 \div \text{final}$ **do**
  % $\mathcal{E}$ was obtained during the computation of the strainline, Section 3.2.1.
  $\mathbf{x}_i^+ = \mathbf{x}_i + \varepsilon \boldsymbol{\xi}_2$
  $\mathbf{x}_i^- = \mathbf{x}_i - \varepsilon \boldsymbol{\xi}_2$
end while
$\gamma^+(t_0) := \{\mathbf{x}_0^+, \cdots, \mathbf{x}_{\text{final}}^+\}$
$\gamma^-(t_0) := \{\mathbf{x}_0^-, \cdots, \mathbf{x}_{\text{final}}^-\}$
$\Lambda_2 := \text{int}(\lambda_2(\Gamma(t_0))/\text{length}(\Gamma(t_0))$
$\Lambda_2^+ := \text{int}(\lambda_2(\gamma^+(t_0))/\text{length}(\gamma^+(t_0))$
$\Lambda_2^- := \text{int}(\lambda_2(\gamma^-(t_0))/\text{length}(\gamma^-(t_0))$
if $\Lambda_2 > \Lambda_2^+$ **and** $\Lambda_2 > \Lambda_2^-$ **then**
  $\Gamma(t_0)$ is an LCS.
end if

3.2.7 Example (The Double Gyre) Using the same example than before, Example 3.1.1, with the filter parameters $l_{\min} = 1$ and $l_f = 0.2$. The repelling LCS are computed with Final Algorithm 3. Figure 3.5 shows the differences between the plot obtained by the computation in this thesis and the plot taken from [5].

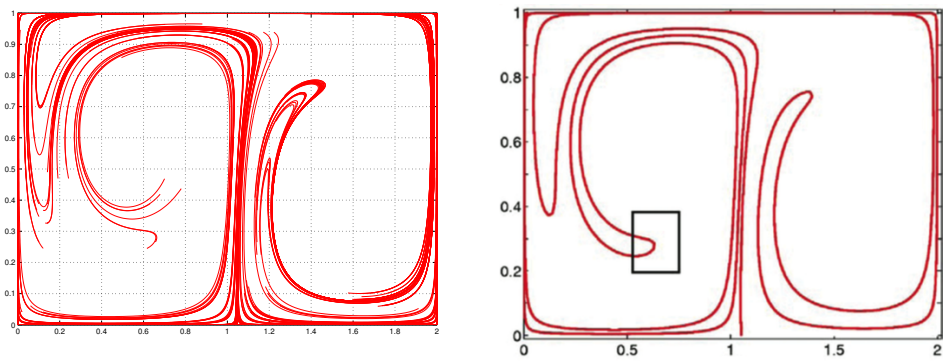

(a) Obtained numerically. (grid: 200×50)

(b) Taken from [5].

Figure 3.5: Repelling LCS of the Double Gyre.

As said many times in this chapter, Figure 3.5 proves that these developed algorithms are very sensitive to numerical errors. In that example, one can see that the results obtained in Figure 3.5a are very similar to those from the literature in Figure 3.5b, but there are many curves shown that shouldn't be. Moreover, the LCS in the square of Figure 3.5b is not completely finished in the numerical obtention of Figure 3.5a. This means that more integration time for the System 3.4 may be needed in order to have longer strainlines.

Even the results given by the Algorithm 3 applied to the Double Gyre do not correspond exactly to those shown in [5], the similarity is clear. The numerical implementation of the LCS theory is very sensitive to the relative and absolute tolerances in the ODE solvers and this has a relevant impact to the computation time because the ODE solver is used many times on any single strainline computation and on any computation of region $\mathcal{U}_0$. Even more, the double linear interpolation implies carrying more numerical errors to the final results. In this thesis, it has been decided to find an equilibria between admissible results and their computation time. More accuracy could have given better results but the time of computation would be too long.

Algorithm 3 LCS-finder inspired by Variational Theory

```
% Referred conditions (A), (B), (C), (D) are those from Proposition 3.2.1.
% G_0 ⊂ Ω is the grid of initial conditions in the phase space.
% [t_0, t_0 + T] is the interval of integration.
% U_0 ⊆ G_0 ⊂ Ω is the set of the grid points that satisfies condition (B).
% ode(f(x_j, t_j), x_j) refers to an ODE solver that returns next point x_{j+1}
% where f(x_j, t_j) is the velocity map of the ODE.
% l_f is the length allowed for (B) failures on strailines (See Section 3.2.1).
% l_min is the minimum length allowed for an LCS.
% length(γ) := Σ_{i=1}^{i=final} ||x_{i-1} − x_i|| computes the length of the curve γ.
for all x_0 ∈ G_0 do
  Check condition (B) %See Section 3.2.2
  if x_0 ∈ U_0 then
    while L < l_f do
      % Find the Cauchy-Green strain tensor Δ(x_0, t_0, T)
      % Computation of strainlines, see Section 3.2.1
      x_{j+1} = ode(ξ̃_1(x_j, s_j), x_j)
      if x_{j+1} ∈ U_0 then
        L := 0
      else
        L := L + ||x_{j+1} − x_j||
      end if
    end while
    if L ≥ l_f then
      It's not an LCS candidate
    else
      LCScand := {x_0, ··· , x_final}
      if length(LCScand) ≥ l_min then
        % Verify condition (D), see Section 3.2.3
        do Algorithm 2
      end if
    end if
  end if
end for
```

3.3 Analogous results of Attracting LCS

Chapter 3 in general is dedicated to the computation of *Repelling LCS*. This section is dedicated to present, briefly, analogous results for *Attracting LCS* in 2−dimensional Dynamical Systems. These last years, 2013 − 2015, researchers have been dedicated to the computation of all kind of LCS, [6].

Recalling Definition 3.2.2 and the fact that an Attracting LCS is a Repelling LCS integrating in backward time, then:

3.3.1 Definition (Stretchline) A *Stretchline* is a strainline integrating ODE 3.4 in backward time.

As in the strainlines, *stretchlines* are the curves of the phase state that present more compressing forces than shearing forces at all points of the curve. Those that present locally most compressing forces than other stretchlines are the *attracting LCS*.

So then, the stretchlines of a Dynamical System form the pattern of the attracting structures of the flow. Finding the stretchlines became easier from 2013 due to this theorem, published and proved in [6].

3.3.2 Theorem

- *Forward time strainlines coincide with backward time stretchlines.*
- *Forward time stretchlines coincide with backward time strainlines.*

From the proof of the Theorem 3.3.2, in Appendix A of [6], the next important corollary is deduced.

3.3.3 Corollary *Given a Dynamical System of the form 1.1 and a finite-time interval $I = [t_0, t_0 + T]$. A stretchline is a curve $\gamma(t_0) \subset \Omega$ such that is the orbit of the next Cauchy problem:*

$$\begin{cases} \boldsymbol{x}'(s) &= \boldsymbol{\xi}_2(\boldsymbol{x}(s), t_0, T) \\ \boldsymbol{x}(0) &= \boldsymbol{x}_0 \in \Omega \\ |\boldsymbol{\xi}_2| &= 1 \end{cases} \tag{3.5}$$

where $\boldsymbol{\xi}_2 = \boldsymbol{\xi}_2(\boldsymbol{x}(s), t_0, T)$ stands for the greatest strain eigenvector calculated at $\boldsymbol{x} \in \Omega$ integrating from t_0 to $t_0 + T$.

This thesis is not going deeper through Attracting LCS. Chapter 4 will use only Repelling LCS. Table 3.6 is a summary of the ODEs that one has to solve in order to find this 2 sets of curves:

Curves	**ODE**
Strainlines	$\mathbf{x}'(s) = \boldsymbol{\xi}_1(\mathbf{x}(s), t_0, T)$
Stretchlines	$\mathbf{x}'(s) = \boldsymbol{\xi}_2(\mathbf{x}(s), t_0, T)$

(3.6)

Those two special curves of the Dynamical System indicate the repelling and attracting structures of the phase space. Evolving them by time, one can have a general idea of the pattern of the flow after a finite-time interval.

Furthermore, Table 3.6 allows the simultaneous construction of attracting and repelling LCS over $I = [t_0, t_0 + T]$ from one single computation. This also makes the backward-time Cauchy-Green strain tensor completely unnecessary.

4 Application to the ER3BP

The objective of this chapter is to apply the concept studied in this thesis, the LCS, to a problem in Astrodynamics. The problem chosen is the computation of *Weak Stability Boundaries* (WSB) in the *Elliptic Restricted Three Body Problem* (ER3BP) which is an important problem in space trajectories design.

First section is dedicated to the definition of the ER3BP and the Weak Stability Boundaries. In second section, the hypothesis and the methodology used are shown and, finally, the results of the application of the LCS theory are shown.

Finally, there is a section dedicated to possible further developments.

4.1 Weak Stability Boundaries

In spacecraft trajectories design, there is one special set of transfers from one planet to another, they are called *low-energy transfers*. These transfers are those which the spacecraft is ballistically captured by the gravitational field of the planet and, thus, propellant is not needed during the capture phase. This technique was used in 1991 when one Japanese satellite, Hiten, reached the Moon using the gravitation forces of the Moon [21].

The technique consists in bringing the spacecraft to a certain point of the space with a certain velocity where it will be captured by the planet. The *Weak Stability Boundaries* (WSB) are separatrices between those points of the space where the spacecraft is captured by the planet and those that escape naturally from the planet.

4.1.1 Elliptic Restricted Three Body Problem

The model taken is the *elliptic restricted three body problem* (ER3BP). In the ER3BP the motion of a massless particle, P_3, is studied under the gravitational field generated by the motion of two masses (the primaries), P_1 and P_2, of masses m_1 and m_2 (with $m_1 >> m_2$) respectively.

As the name says, the elliptic problem models the motion of P_2 around P_1 as elliptic trajectories instead of circular, as shown in the schematic Figure 4.1.

Their relative distance will therefore vary depending on the point in which P_2 is found in its elliptic orbit around P_1, [21]. The solution of the two-body problem relative to $P_1 - P_2$ motion gives their distance, r:

$$r(f) = \frac{a(1-e^2)}{1+e\cos f} \tag{4.1}$$

a being the semi-major axis of the orbit of P_2 around P_1, e its eccentricity and f the true anomaly as can be seen in Figure 4.1.

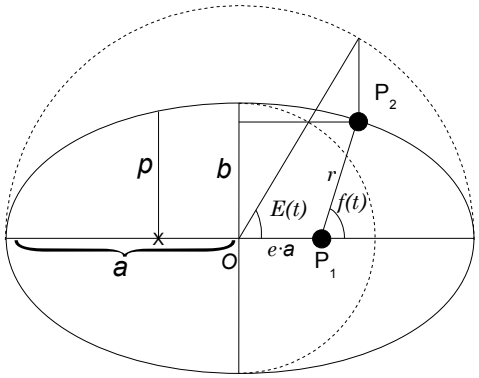

Figure 4.1: Elliptic orbit of P_2

The equations that describe the motion of the particle P_3, relative to the normalized co-rotating frame, under the gravitational field generated by the elliptic motion of the primaries, are, [21]:

$$\begin{cases} x'' - 2y' = \dfrac{\partial \omega}{\partial x} \\ y'' + 2x' = \dfrac{\partial \omega}{\partial y} \end{cases} \tag{4.2}$$

In this case, the derivates in the left term of the equations are not temporal, as there is a new independent variable that plays the role of time in the elliptic problem, the true anomaly, f. In the right terms of (4.2) appear the partial derivates of the potential, ω, given by:

$$\omega(x, y, f) = \frac{\Omega(x, y)}{1 + e_p \cos f},$$

being e_p the eccentricity of P_2 orbit around P_1 and Ω the potential function defined as follows:

$$\Omega(x, y) = \frac{1}{2}\left(x^2 + y^2\right) + \frac{1-\mu}{r_1} + \frac{\mu}{r_2} + \frac{1}{2}\mu(1-\mu)$$

where $r_1 = \sqrt{(x+\mu)^2 + y^2}$ and $r_2 = \sqrt{(x+\mu-1)^2 + y^2}$ represent the distances from P_3 to P_1 and P_2 respectively, as in the scheme of Figure 4.2. On the other hand, $\mu = \frac{m_2}{m_1+m_2}$ is the mass parameter.

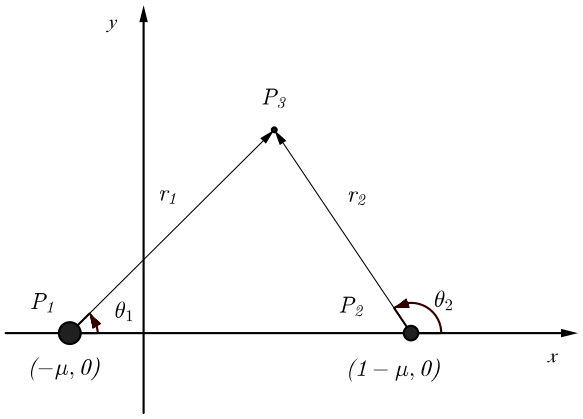

Figure 4.2: Elliptic orbit

The dependence of the true anomaly on time is, [11, 12]:

$$\frac{df}{dt} = \frac{(1 + e_p \cos f)^2}{(1 - e_p^2)^{3/2}}$$

12 Remark The study of the ballistic capture trajectories involves orbits that can result in collision of P_3 with either P_1 or P_2. This fact implies a fail in the numerical integration as there is a singularity in the System 4.2 when $r_{1,2} \to 0$. It is convenient therefore to regularize the equations of motion in the vicinities of this limit, the regularization of Levi-Civita presents fairly good solutions to the problem. Further details of Levi-Civita methods can be found in [21].

4.1.2 Weak Stability Boundaries

Before explaining the meaning of stable sets and their computation it is important to define *ballistic capture*. As mentioned in [14], *ballistic capture by a planet occurs when an object enters, under natural dynamics, within the sphere of influence of that planet and makes at least one complete revolution around it.* This means that, in ballistic capture, additional energy does not need to be provided to the object and, therefore, no propellant has to be used in the maneuver. This savings of propellant can be useful later, for example, to stabilize the orbit once the satellite has been captured by the planet.

In the ER3BP the Kepler energy of the particle P_3 relative to P_2, which is the mechanical energy (kinetic and potential) of particle P_3 considering only P_2 attraction, can be written as:

$$H_2(f) = \frac{1}{2} v_2^2(f) - \frac{\mu}{r_2} \tag{4.3}$$

where v_2 is the speed of P_3 relative to a P_2-centered inertial reference frame. In polar coordinates it is expressed by:

$$v_2^2(f) = \left(\frac{r_2 e_p \sin f}{1 + e_p \cos f} r_2' \right) + r_2^2 (1 + \cos \theta_2')^2 \tag{4.4}$$

4.1.1 Definition (Ballistic Capture) Based on this Kepler energy, and considering $\mathbf{x}(f)$ as a solution of (4.2), it is possible to define:

(a) *Ballistic Capture*: P_3 is ballistically captured by P_2 at f_1 if $\mathrm{H}_2(\mathbf{x}(f_1)) < 0$, and it is temporarily ballistically captured (or weakly captured) by P_2 if $\mathrm{H}_2(\mathbf{x}(f)) < 0$ for $f_1 \leq f \leq f_2$ and $\mathrm{H}_2(\mathbf{x}(f)) > 0$ for $f < f_1$ and $f > f_2$, for finite anomalies $f_1 < f_2$.

(b) *Ballistic Escape*: P_3 is ballistically ejected (or ballistically escapes) from P_2 at f_1 if $\mathrm{H}_2(\mathbf{x}(f)) < 0$, for $f < f_1$ and $\mathrm{H}_2(\mathbf{x}(f)) \geq 0$ for $f \geq f_1$.

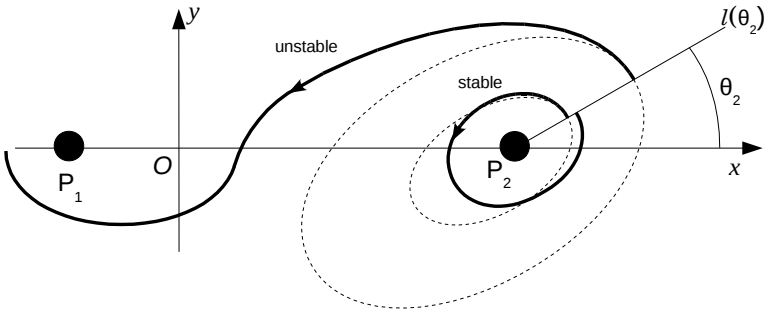

Figure 4.3: 1−stable and 1−unstable trajectories

To verify the ballistic capture, the revolutions of P_3 around P_2 are tracked. For this reason, the trajectories with the following characteristics will be studied:

1) The initial position of the third particle P_3 is on a radial segment $l(\theta_2)$ departing from P_2 and making an angle θ_2 with the x-axis of the synodic dimensionless reference system. The trajectory is assumed to start at the periapsis of an oscullating ellipse around P_2, whose semimajor axis lies on $l(\theta_2)$ and whose eccentricity e is fixed along $l(\theta_2)$. Thus, the initial distance from P_2 is given by:

$$r_2(f_0) = a(1 - e) \tag{4.5}$$

where a and e are the major axis and the eccentricy of the ellipse orbit of P_3 around P_2.

2) In the P_2-centered frame the initial velocity of the particle is perpendicular to $l(\theta_2)$ and, as P_3 is on the periapsis of its oscullating ellipse, the initial Kepler energy is always negative, $H_2(f_0) < 0$. In [11], the initial velocity of P_3 is given by the map $\mathcal{M} : \mathbb{R}^2 \to \mathbb{R}^4$:

$$\mathcal{M}(r,\theta) = \begin{cases} r_2 = r \\ \theta_2 = \theta \\ r_2' = \dfrac{re_p \sin(f_0)}{1 + e_p \cos(f_0)} \\ \theta_2' = \sqrt{\dfrac{\mu(1+e)}{r^3(1+e_p\cos(f_0))}} - 1 \end{cases} \tag{4.6}$$

3) Once P_3 leaves the initial position on $l(\theta_2)$, the equations of the ER3BP can be integrated. According to the definition of ballistic capture and as can be seen in Figure 4.3, the motion is said to be *n-stable* if P_3 makes n turns around P_2 and returns to $l(\theta_2)$ on a point where its Kepler energy relative to the smaller primary is negative, without having completed any revolution about P_1 along this trajectory. Otherwise the motion is said to be *n-unstable*. These can occur either if P_3 makes at least one revolution about P_1 (this situation is called *primary interchange escape*) or if it returns to $l(\theta_2)$ with $H_2 > 0$ after having done n revolutions about P_2.

4.1.2 Definition ($n-$stable sets) Given an ER3BP system with the fixed parameters e, f_0, fixed an angle $\theta_2 \in [0, 2\pi]$, let $l(\theta_2)$ be the radial segment, the *n-stable set* on $l(\theta_2)$ is defined as the countable union of open intervals:

$$\mathcal{W}_n(\theta_2, e, f_0) = \bigcup_{k \geqslant 1} \left(r^*_{2k-1}, r^*_{2k}\right), \tag{4.7}$$

with $r^*_1 = 0$. Excepting r^*_1, the points r^*_{2k}, the upper limits of the intervals, are $n-$unstable.

If these sets are computed for each value of θ_2 and fixed (e, f_0), it is obtained:

$$\mathcal{W}_n(e, f_0) = \bigcup_{\theta_2 \in [0,2\pi]} \mathcal{W}_n(\theta_2, e, f_0), \tag{4.8}$$

and finally, if $\mathcal{W}_n(e, f_0)$ are computed for a fixed value of eccentricity e, the *complete n-stable set* is given by:

$$\mathcal{W}_n(f_0) = \bigcup_{e \in [0,1)} \mathcal{W}_n(e, f_0). \tag{4.9}$$

13 Remark Note that

$$\mathcal{W}_n(e, f_0) \subseteq \cdots \subseteq \mathcal{W}_2(e, f_0) \subseteq \mathcal{W}_1(e, f_0)$$

Now it is possible to define the Weak Stability Boundary (WSB) of order n that contains the set of points $r^*(\theta_2, e)$ along $l(\theta_2)$ in which there is a change of the stability of the trajectory.

4.1.3 Definition (Weak Stability Boundary (WSB)) Given an ER3BP system with a fixed true anomaly, f_0. The *Weak Stability Boundary (WSB)* is the locus of all points $r^*(\theta, e)$, for all radial lines $l(\theta_2)$, at which there is a change of stability of the initial trajectory. r^* represents one of the endpoints of an interval (r^*_{2k-1}, r^*_{2k}), characterized by the fact that any $r \in (r^*_{2k-1}, r^*_{2k})$ gives a n-stable trajectory, and there exist $r' \notin (r^*_{2k-1}, r^*_{2k})$ arbitrarily close to either r^*_{2k-1} or r^*_{2k} that give a n-unstable solution. Its formal expression is:

$$\partial \mathcal{W}_n(f_0) = \{r^*(\theta_2, e) | \theta_2 \in [0, 2\pi], e \in [0, 1)\} \tag{4.10}$$

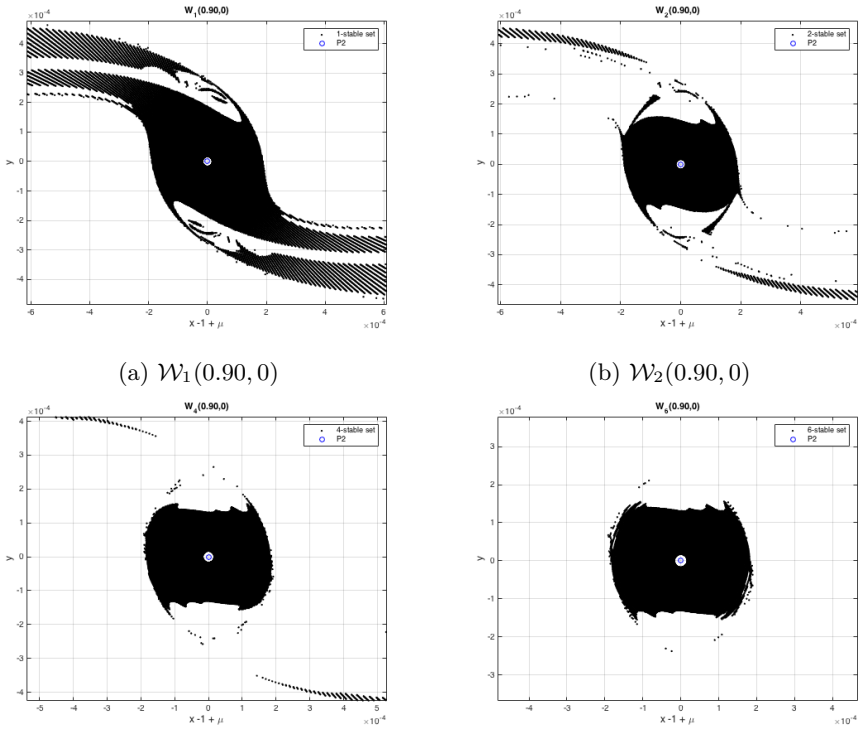

(a) $\mathcal{W}_1(0.90, 0)$ (b) $\mathcal{W}_2(0.90, 0)$

(c) $\mathcal{W}_4(0.90, 0)$ (d) $\mathcal{W}_6(0.90, 0)$

Figure 4.4: $n-$stable sets of the Sun-Mars system. These graphs were obtained with the Data sets computed by the authors of [11].

Figure 4.4 shows some $n-$stable sets, in particular, the $n-$stable points of the Sun-Mars system are represented in black, for $n = 1, 2, 4, 6$. The boundaries of the black sets are the $n-$WSB of the system, i.e. $\partial \mathcal{W}_1(0.90, 0)$, $\partial \mathcal{W}_2(0.90, 0)$, $\partial \mathcal{W}_4(0.90, 0)$ and $\partial \mathcal{W}_6(0.90, 0)$ respectively.

4.2 Adaptation to LCS Theory

The numerical method for obtaining the WSB is a hard computation. In [11], the method is explained in depth. It consists in doing a grid $\mathcal{G}$ nearby P_2 and integrate the ER3BP system for all points of the form $(r_2, \theta_2) \in \mathcal{G}$, Equations 4.2, longer enough to check if the particle returns to $l(\theta_2)$ doing at least one revolution around P_2. If it does, it will be called $1-$stable, if it does a full turn around the other body, P_1, it is called $1-$unstable. Furthermore, for the sets $\mathcal{W}_n(e, f_0)$ with $n > 1$, the computation is even more expensive because one has to integrate until the particle does at least n revolutions around P_2.

4.2.1 Hypothesis

The LCS theory is applied in this problem in order to reduce the computational time of computing the WSB and also to have a better understanding of the qualitative motion around P_2. The idea is to use *repelling LCS* for their characteristic of being separatrices of qualitative different dynamics because particles that are ballistically captured have different dynamics from those that escape from the attraction of P_2.

In Figure 4.5, the orbit of three particular particles from $l(\theta_2 = 0)$ around P_2 are plotted. The red one belongs to a point from the set $\mathcal{W}_1(0.90, 0)$ near to the boundary, the pink one to one point from the boundary $\partial\mathcal{W}_1(0.90, 0)$ and the blue one belongs to a point from the outside of the $1-$stable set. These three near points have qualitatively different dynamics, the red one returns, the blue one escapes and the pink acts as a separatrix between these two dynamics.

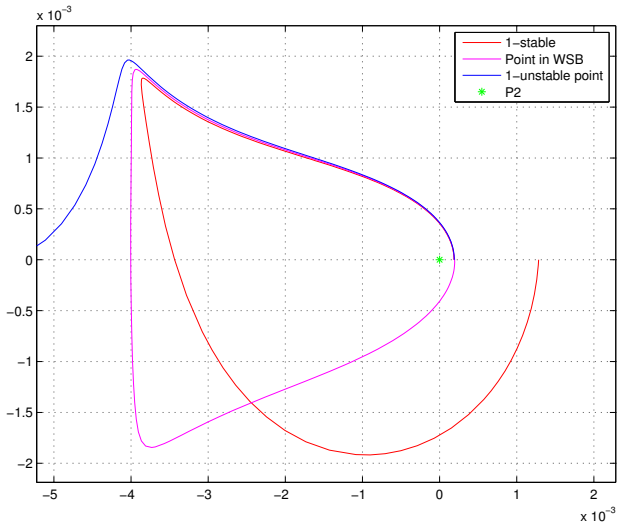

Figure 4.5: Different dynamics of 3 particles

Qualitatively, it is easy to appreciate the different dynamics between the red orbit and the blue orbit. So then, it is natural to think that the WSB should be a *repelling LCS* of the system, due to their separatrix property. The objective of chapter 4 is to

prove computationally that one *repelling LCS* of the system is the boundary of the 1−stable set.

4.2.2 The system

Equations 4.2 for the motion of P_3 in the ER3BP can be re-written of the form:

$$\begin{cases} x' &= v_x \\ y' &= v_y \\ v_x' &= 2v_y + \dfrac{\partial \omega}{\partial x} \\ v_y' &= -2v_x + \dfrac{\partial \omega}{\partial y} \end{cases} \tag{4.11}$$

This 4−dimensional ODE system can be solved by any ODE solver. Furthermore, one can obtain also the Jacobian of the flow integrating the Variational equations, as done in Chapter 3. In that case, the Variational Equations is a $n + n^2 = 4 + 4^4 = 20$ ODE system.

The flow of the Dynamical System studied in the WSB problem is ψ, that can be expressed as the composition of functions that follows. This chain of transformations is a 2−dimensional Dynamical System, so algorithms and results from Chapter 3 can be used.

$$\begin{array}{ccccccccccc} & & & & & & \psi & & & & \\ & & \curvearrowright & & & & & & \curvearrowright & & \\ \mathbb{R}^2 & \xrightarrow{\mathcal{M}} & \mathbb{R}^4 & \xrightarrow{\text{P2C}} & \mathbb{R}^4 & \xrightarrow{\varphi} & \mathbb{R}^4 & \xrightarrow{\text{C2P}} & \mathbb{R}^4 & \xrightarrow{\pi} & \mathbb{R}^2 \\ \begin{Bmatrix} r_i \\ \theta_i \end{Bmatrix} & \mapsto & \begin{Bmatrix} r_i \\ \theta_i \\ r_i' \\ \theta_i' \end{Bmatrix} & \mapsto & \begin{Bmatrix} x_i \\ y_i \\ x_i' \\ y_i' \end{Bmatrix} & \mapsto & \begin{Bmatrix} x_f \\ y_f \\ x_f' \\ y_f' \end{Bmatrix} & \mapsto & \begin{Bmatrix} r_f \\ \theta_f \\ r_f' \\ \theta_f' \end{Bmatrix} & \mapsto & \begin{Bmatrix} r_f \\ \theta_f \end{Bmatrix} \end{array} \tag{4.12}$$

where:

- $\mathcal{M}$ is the map defined in System 4.6. This map converts the phase space which has dimension 2 to a 4−dimensional phase space. It determines the velocity of the particle P_3 at the initial time, always perpendicular to $l(\theta_2)$ and such that $H_2(f_0) < 0$.
- P2C is a changing references function from Polars centered in P_2 to Cartesian reference:

$$\text{P2C}(r_0, \theta_0, r_0', \theta_0') = \begin{cases} x_0 = 1 - \mu + r_0 \cos(\theta_0) \\ y_0 = r_0 \sin(\theta_0) \\ x_0' = r_0' \cos(\theta_0) - r_0 \theta_0' \sin(\theta_0) \\ y_0' = r_0' \sin(\theta_0) + r_0 \theta_0' \cos(\theta_0) \end{cases}$$

- φ is the flow of the ER3BP, described by Equations 4.11.
- C2P is the inverse of P2C, so it changes the reference system from Cartesian to Polars centered in P_2.
- π is the projection of $\mathbb{R}^4$ to $\mathbb{R}^2$, $\pi(r_f, \theta_f, r_f', \theta_f') = (r_f, \theta_f)$.

ψ is the flow of a $2-$dimensional dynamical system. Therefore, Algorithm 3 can be applied in order to find the repelling LCS of the phase space. The Cauchy-Green strain tensor of this system is $\Delta = \Psi^T \Psi$ where $\Psi = \frac{D\psi}{\partial r \partial \theta}(r_i, \theta_i)$ is the Jacobian of the flow $\psi := \pi \circ \text{C2P} \circ \phi \circ \text{P2C} \circ \mathcal{M}$, that can be computed using the chain rule.

The Jacobian of the flow of the ER3BP, Φ, is computed numerically using the Variational Equations. By contrast, all the other Jacobians are calculated by formal derivation.

4.2.3 Methodology

Due to the objective of this chapter, that is to demonstrate that the borders of the $1-$stable set are repelling LCS, the algorithm used is quite different to Algorithm 3 from chapter 3. In this case, the grid of the phase space is not needed. The idea is to solve System 3.4 from an initial condition in $\partial \mathcal{W}_1(e, f_0)$ as shown in Algorithm 4. Then, one has to check if the strainline obtained satisfies conditions (B) and (D) of Proposition 3.2.1.

In this case, $\theta_2 = 0$ and the parameters for the Sun-Mars system, taken from [11], have been chosen:

- Sun mass: $m_1 = 1.989 \cdot 10^{30}$ Kg.
- Mars mass: $m_2 = 6.41693 \cdot 10^{23}$ Kg.
- Mass parameter: $\mu = \frac{m_2}{m_1 + m_2} = 3.226208 \cdot 10^{-7}$.
- Eccentricity of Sun-Mars system: $e_p = 0.093418$.
- Eccentricity of orbit of P_3: $e = 0.90$.
- Initial true anomaly: $f_0 = 0$.

Furthermore, the filtering parameters considered in Chapter 3, used to soften the numerical errors effect are $l_{\min} = 0.2$ and $l_f = l_{\min}/15 = 0.0133$.

Algorithm 4 WSB-finder using LCS Theory

```
% Referred conditions (A), (B), (C), (D) are those from Proposition 3.2.1.
% ode(f(x_j, t_j), x_j) refers to an ODE solver that returns next point x_{j+1}
% where f(x_j, t_j) is the velocity map of the ODE.
% l_f is the length allowed for (B) failures on strailines (See Section 3.2.1).
% l_min is the minimum length allowed for an LCS.
% length(γ) := Σ_{i=1}^{i=fin} ‖x_{i-1} − x_i‖ computes the length of the curve γ.
Given θ_2 ∈ [0, 2π] fixed.
Find x_0 := (r*, θ_2) ∈ ∂W_1(e, f_0)
if x_0 ∈ U_0 then
  while L < l_f do
    % Find the Cauchy-Green strain tensor Δ(x_0, t_0, T)
    % Computation of strainlines, see Section 3.2.1
    x_{j+1} = ode(ξ̃_1(x_j, s_j), x_j)
    if x_{j+1} ∈ U_0 then
      L := 0
    else
      L := L + ‖x_{j+1} − x_j‖
    end if
  end while
  if L ≥ l_f then
    It's not an LCS candidate
  else
    LCScand := {x_0, ··· , x_fin}
    if length(LCScand) ≥ l_min then
      % Verify condition (D), see Section 3.2.3
      do Algorithm 2
    end if
  end if
end if
```

4.3 Results and Analysis

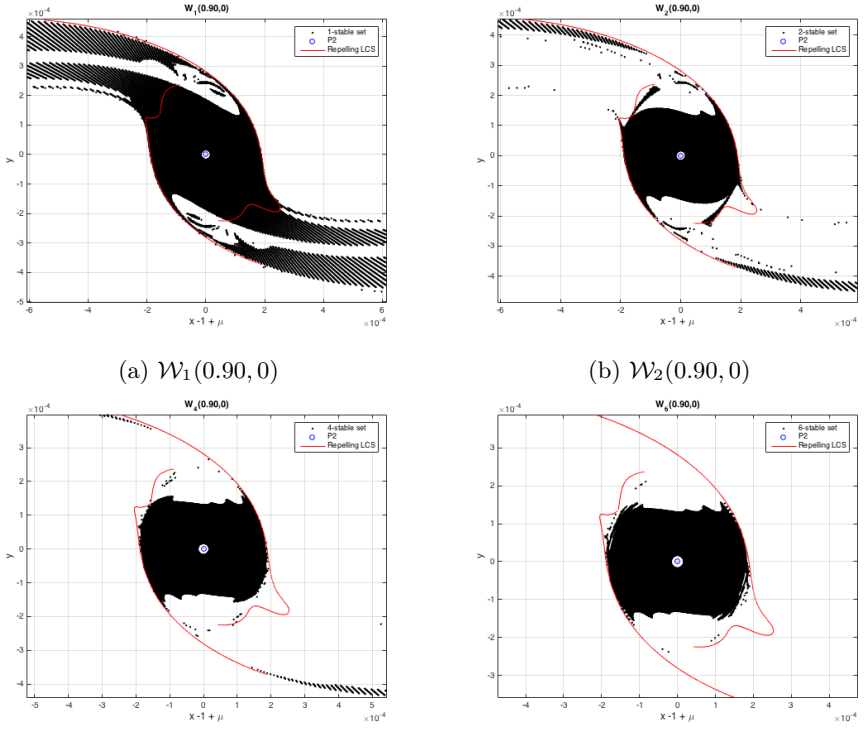

(a) $\mathcal{W}_1(0.90, 0)$ (b) $\mathcal{W}_2(0.90, 0)$

(c) $\mathcal{W}_4(0.90, 0)$ (d) $\mathcal{W}_6(0.90, 0)$

Figure 4.6: $n-$stable sets of the Sun Mars system.

Figure 4.6 shows the strainlines computed beginning at $\theta_2 = 0$ and $\theta_2 = \pi$. As explained in Section 4.2.3, conditions (B) and (D) of Proposition 3.2.1 have been checked for all points of the integration of the strainline. Thus, the red curves in Figure 4.6 are the Repelling LCS of the ER3BP over $[0, f_{\text{final}}]$.

In this first experimentation, the initial conditions are taken from the Data sets computed by *F. Topputo* and *N. Hyeraci* in $2010 - 2013$ with their method explained in [11, 12]. The points from the boundary of $\mathcal{W}_1(0.90, 0)$ chosen are $(r^*, \theta^*) = (1.882295326, 0)$ and $(r^*, \theta^*) = (1.882295326, \pi)$. For these points, the final true anomaly of integration are $f_{\text{final}} = 2.9332364420$ and $f_{\text{final}} = 2.4847866565$ respectively, which are the returning true anomalies of the points (r^*, θ^*)[1].

In figure 4.6a, the $1-$stable set, $\mathcal{W}_1(0.90, 0)$, and the repelling LCS obtained by Algorithm 4 are plotted. Note that the repelling LCS are the boundaries of the set at the right in the left wing of the set and at the left in the right wing, as expected. Surprisingly, the LCS does not trace the boundary at the other sides of the wings, as seen in zoomed Figure 4.7.

[1]The *returning true anomaly* is the true anomaly of the particle when it has returned to $l(\theta^*)$ after at least one revolution.

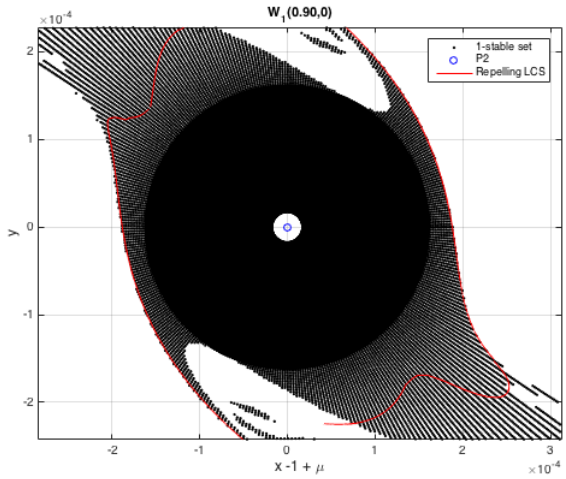

Figure 4.7: $\mathcal{W}_1(0.90, 0)$ and repelling LCS.

In Figure 4.8, there are plotted the orbits of two pairs of points. Blue and pink trajectories are the orbits of two nearby points in $\mathcal{W}_1(0.90, 0)$ that are separated by the repelling LCS. The orbits are integrated from $f_0 = 0$ to $f_{\text{final}} = 2.4847866565$, like the invariants of $\Delta(\mathbf{x}_0, f_0, f_{\text{final}})$. Qualitatively, one can easily see that their trajectories are similar at the beginning but they finally diverge.

Analogously, there occurs the same with the green and light blue trajectories. At the beginning they are very similar but they start to diverge and finally are completely different. This fact justifies that the repelling LCS cross between the two initial points. As stated at the beginning of this thesis, the repelling LCS act as separatrices of different dynamics in the phase state.

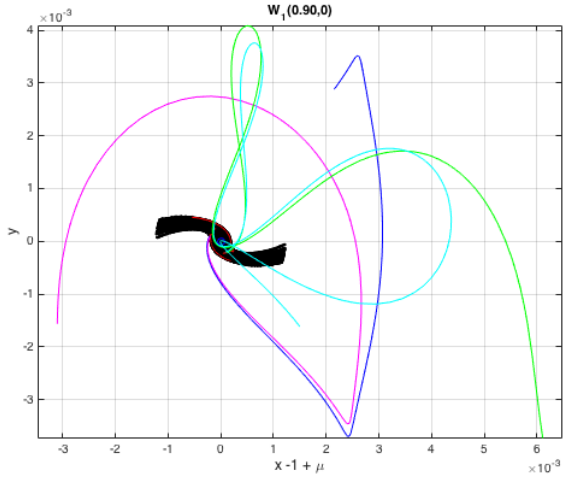

Figure 4.8: Orbits of 4 points in $\mathcal{W}_1(0.90, 0)$.

In conclusion, repelling LCS consider different dynamics also in the stable set. So,

even though the computed strainlines traced the boundary in some areas, they are not distinguishing the unstable set from the stable set for all points of the line. Repelling LCS are more sensitive to the different dynamics of the particles than considered in the hypothesis, Section 4.2.1.

4.4 Future Developments

The preliminary results obtained in Chapter 4 of this thesis are a brand-new results in the field of the WSB. This new experimental method to find the *Weak Stability Boundaries* of an ER3BP system is more efficient computationally. The results presented give a new tool that can be exploited. On the other hand, some questions are opened and must be considered for further research in this way:

1) To find, with a fixed f_{final}, if there are more repelling LCS in the phase state. This computation might be longer, a complete radial grid of the phase space around P_2 must be built and one should run Algorithm 3.

   In that case, check what they do really separate in the phase space.

   In this chapter, it has only been checked if the repelling LCS obtained from a boundary point were WSB.

2) The final true anomaly, f_{final}, for the invariants $\mathcal{E} = \{\lambda_1, \lambda_2, \boldsymbol{\xi}_1, \boldsymbol{\xi}_2\}$ of the finite-time Cauchy-Green strain tensor. As said in Definition 2.3.5, one material surface is a *Repelling LCS* over a finite interval.

   In this chapter, the returning true anomaly has been considered as f_{final}, but further analysis must check what happens at longer and shorter integrations.

   Furthermore, every $n-$stable points has his own returning true anomaly, so it's natural to consider true anomaly variations in the phase space in next experiments.

3) Extension of the hypothesis and experiments done in $\mathcal{W}_1(e, f_0)$ to $\mathcal{W}_n(e, f_0)$, $n > 1$. One can check if repelling LCS using the returning true anomalies for the $n-$th revolution are also the WSB of the $\mathcal{W}_n(e, f_0)$.

4) The inherent condition of negative Kepler energy at the returning point in the construction of the $n-$stable sets does not affect to the trajectory of the particle. Further research can also be directed to find out if there's some relation between this condition and the repelling LCS or if this condition can be dropped from the WSB direction.

5) Find under which conditions can the LCS theory be useful to separate the two dynamics (stable and unstable) in the ER3BP. The ER3BP is a very studied problem in Aerospace Engineering to calculate interplanetary transfers or to optimize the propellant used, for example. Therefore, a new field of research can be opened, researchers can orient their work to state specific results of LCS theory in the ER3BP, so the application of that results can improve the techniques used in trajectories design.

5 Conclusions

In this work, a review of the Lagrangian Coherent Structures in non-linear Dynamical Systems has been done. The first objective of this thesis was to understand this new topic which is being used in unsteady fluid dynamics during this last decade. A literature review has been done and shown in Chapter 2. Two different theories have been studied, the FTLE field and the Variational LCS theory, in order to understand the evolution of this topic research during these last years. One concludes that LCS are a very promising tool to predict future situations of chaotic dynamical systems.

After this theoretical research, this thesis presents an algorithm to find the LCS of a $2-$dimensional Dynamical System. One should remark the difficulty to find accurate results due to numerical errors. These algorithms use several times ODE and eigenvalue solvers consecutively and numerical differentation. Furthermore, it is very important to find an equilibrium between the computation time and the accuracy of the results obtained. Computations of these algorithms are very expensive in time and memory and very sensitive to the accuracy demanded.

One last objective of this thesis was to find an application of this tool in Aerospace Engineering. For this reason, the Elliptic Restricted Three Body Problem has been studied and some hypotheses linking the repelling LCS and the Weak Stability Boundaries (WSB) have been presented. A new methodology, based on algorithms shown in Chapter 3, has been designed in order to find the WSB of the Sun-Mars system.

The results obtained by using the LCS theory are promising and the computation by this new method is faster than the method presented in [11]. Using repelling LCS to separate the particles that are ballistically captured by Mars and the ones that escapes from it could be a new technique in space trajectories design.

Despite these promising preliminary results, a lot of questions are open in this problem, such as the exact value of the final true anomaly for the integrations or the Kepler energy condition in the ballistic capture. More research in that direction has to be done in order to state when the repelling LCS of the ER3BP are the boundaries of the stable set.

Finally, the results presented in this thesis on the WSB problem add importance to LCS as a new tool in non-linear dynamical systems. Researchers of this topic remarked in some informative articles such as [18] the relevance that LCS theory has in the study of unsteady flows. The new application presented opens the range of dynamical systems where they can be applied.

References

[1] `http://mathworks.com/matlabcentral/fileexchange/13490-adaptive-robust-numerical-differentiation/content/DERIVESTsuite/hessian.m`, December 2014.

[2] E. Belbruno, M. Gidea, and F. Topputo. Weak stability boundary and invariant manifolds. *SIAM J. Applied Dynamical Systems*, (3):1061–1089, 2010.

[3] D. Blazevski and G. Haller. Hyperbolic and elliptic transport barriers in three dimensional unsteady flows. *Physica D*, (273–274):46–62, 2014.

[4] M. Farazmand and G. Haller. Erratum and addendum to "A variational theory of hyperbolic lagrangian coherent structures". *Physica D*, (241):439–441, 2011.

[5] M. Farazmand and G. Haller. Computing lagrangian coherent structures from their variational theory. *Chaos*, (22):1–12, 2012.

[6] M. Farazmand and G. Haller. Attracting and repelling lagrangian coherent structures from a single computation. *Chaos*, (23):023101, 2013.

[7] G. Haller. Distinguished material surfaces and coherent structures in three-dimensional fluid flows. *Physica D*, (149):248–277, 2000.

[8] G. Haller. A variational theory of hyperbolic lagrangian coherent structures. *Physica D*, (240):574–598, 2010.

[9] G. Haller. Lagrangian coherent structures. *The Annual Review of Fluid Mechanics*, (47):134–161, 2015.

[10] G. Haller and G. Yuan. Lagrangian coherent structures in two-dimensional turbulence. *Physica D*, (147):352–370, 2000.

[11] N. Hyeraci and F. Topputo. Method to design ballistic capture in the elliptic restricted three-body problem. *Journal of Guidance, Control and Dynamics*, (6):1814–1823, 2010.

[12] N. Hyeraci and F. Topputo. The role of true anomaly in ballistic capture. *Celest Mech Dyn Astr*, (116):175–193, 2013.

[13] D. H. Kelley, M. R. Allshouse, and N. T. Ouellette. Lagrangian coherent structures separate distinct regions in fluid flows. *Physical Review*, (88):1–4, 2013.

[14] W. S. Koon, M. W. Lo, J. E. Marsden, and S. D. Ross. Low energy transfer to the moon. *Celestial Mechanics and Dynamical Astronomy*, (81):63–73, 2001.

[15] F. Leiken, S. C. Shadden, and J. E. Marsden. Lagrangian coherent structures in n-dimensional systems. *Journal of Mathematical Physics*, (48):1–19, 2007.

[16] F. Lekien and N. Leonard. Dynamically consistent lagrangian coherent structures. *Experimental Caos*, (742):132–139, 2004.

[17] J. Meiss. Dynamical systems. 2(2):1629, 2007.

[18] T. Peacock and G. Haller. Lagrangian coherent structures: The hidden skeleton of fluid flows. *Physics Today*, (66):41–47, 2013.

[19] A. Quarteroni and F. Saleri. *Introduzione al Calcolo Scientifico - Esercizi e problemi risolti con MATLAB*. Politecnico di Milano, Milano, Italy, 2006.

[20] S. C. Shadden, F. Lekien, and J. E. Marsden. Definition and properties of lagrangian coherent structures from finite-time lyapunov exponents in two-dimensional flows. *Physica D*, (212):271–304, 2005.

[21] F. Topputo and E. Belbruno. Computation of weak stability boundaries: Sun – Jupiter. *Celest Mech Dyn Astr*, (105):3–17, 2009.